DASA 2508

DEVELOPMENT OF A HIGH-SENSITIVITY PIEZORESISTIVE SHOCK TRANSDUCER FOR THE LOW KILOBAR RANGE

Final Report

By

DOUGLAS D. KEOUGH

March 25, 1970

DEFENSE ATOMIC SUPPORT AGENCY
WASHINGTON, D.C. 20301

STANFORD RESEARCH INSTITUTE
MENLO PARK, CALIFORNIA 94025

DASA-69-C-0014

Final Report

DASA 2508

March 25, 1970

DEVELOPMENT OF A HIGH-SENSITIVITY PIEZORESISTIVE SHOCK TRANSDUCER FOR THE LOW KILOBAR RANGE

By: DOUGLAS D. KEOUGH

Prepared for:

SHOCK PHYSICS DIRECTORATE
DEFENSE ATOMIC SUPPORT AGENCY
WASHINGTON, D.C. 20305

CONTRACT DASA-69-C-0014

SRI Project 7511

This work was supported by the Advanced Research Project Agency under ARPA Order 1238 PC 8F10, Program Code 7B42-71107.

Approved:

G. R. ABRAHAMSON, *Director*
Poulter Laboratory

ABSTRACT

The shock piezoresistance response of two metals, ytterbium and bismuth, was investigated--ytterbium over a range from 4 to 40 kbar and bismuth at 10 and 20 kbar. The sensitivity of both materials at a few kilobars is approximately 12 times that of manganin and both show nonlinear, monotonically varying resistance-stress behavior. Unloading response was measured at from 10 and 20 kbar in ytterbium and found to be nonlinear at the higher range. A positive residual resistance was measured which was essentially independent of peak stress. A system consisting of the impact of two elastic materials was developed for the measurement of hysteresis. Additional hysteresis and low-kilobar data are needed to describe the response fully.

Comparison of static and dynamic piezoresistance data indicates that the difference between the two is too large to be attributed to temperature and geometrical considerations. Although it may be due to defect production, this phenomenon was not investigated specifically. Results with manganin, foils and wires, however, did show a difference in certain insulators which is attributed to defect production.

Foils approximately 0.013 mm thick and films approximately 0.6 μ thick were constructed readily from bulk ytterbium. Bismuth films were constructed from bulk bismuth by vapor deposition.

Long-time-duration recording was achieved by bonding ytterbium foils between wafers of polycrystalline aluminum oxide. A duration of $\sim$ 30 μsec at a stress of 10 kbar was achieved in experiments with the SRI 4-inch barrel diameter gas gun. Reduction in foil elongation and hence a reduction in sensitivity to lateral stress disturbances appears to be due to the encapsulation of the foil in high-modulus, high-shock-impedance insulators. Further tests of this concept should be performed in <u>in situ</u> experiments.

PREFACE

The author would like to express appreciation to Paul De Carli for assistance with the metallurgical aspects of the program and to Messrs. F. Medlong, W. McCord, L. Hall, and A. Bartlett for technical support.

CONTENTS

ILLUSTRATIONS

ILLUSTRATIONS (Concluded)

TABLES

1. INTRODUCTION

The behavior of rocks and soils under shock compression is of great interest to a wide variety of weapon effects programs and to many PLOWSHARE programs. Significant in the measurement of the behavior of these materials is the variation of the stress-time profile of a shock-induced compression wave as it travels through the rocks and soils. Close to the source of an input pulse the stresses are well above material strengths. In this stress regime, the plastic behavior is dominant. At larger distances, the stress has attenuated to an elastic and plastic wave and at still larger distances to the elastic wave only. It is this elastic wave of many hundreds of microseconds duration that is of interest to the structures designers and to the geologist. The amplitude may be from a fraction to tens of kilobars and the duration from hundreds to thousands of microseconds.

The objective of the work discussed in this report is the development of high-sensitivity piezoresistive transducers capable of being imbedded in rocks and soils and of recording low-amplitude stresses for long recording durations.

In the present investigation, the two major problems associated with the use of manganin piezoresistance field gages, namely low sensitivity and insufficient recording duration, have been studied by:

(1) Investigating other metals as possible sensors

(2) Investigating methods of encapsulating the sensor to prevent early gage failure.

The following sections discuss considerations, techniques, results, and conclusions of the investigation of other piezoresistance metals and sensor encapsulation.

2. BACKGROUND

Piezoresistive transducer systems for use in soils and rocks have been developed[1,2] which use manganin grids imbedded in epoxies or, where conditions permit, directly in the soil or rock. These systems have been used in numerous field tests[3-8] to record stress profiles ranging from a few kilobars to hundreds of kilobars at durations on the order of 100 to 35 μsec, respectively. However, the stress-resistance sensitivity of manganin, $0.29 \pm 0.01 \times 10^{-2}$ Ω/Ω kbar, is marginally adequate for the low kilobar and subkilobar regions in the field environments encountered. Higher sensitivity nonmetallic piezoresistive materials have been used as stress sensors, notably liquids and semiconductors.[9] In general these materials exhibit as large a change in resistance with shock temperature as with shock stress and therefore stress-time information derived from a resistance-time measurement made with these materials is dependent on knowledge of their temperature-time history. Corrections for temperature are derived from calculation of the pressure-volume-temperature (P-V-T) equation of state or from measurement of the resistance-stress response for an assumed input.

Efforts to find a more sensitive metallic piezoresistive material for labroatory gages have led to the use of calcium and lithium, which possess dynamic piezoresistive coefficients of 0.24×10^{-1} Ω/Ω kbar[10,11] or approximately eight times that of manganin. The coefficients have been found to be constant over the range tested, approximately 10 to 50 kbar. In the range of a few kilobars and less, several other materials are likely candidates (based on static piezoresistance data) for even higher sensitivity sensors. Primary among these are ytterbium, strontium, and bismuth. These materials together with lithium and calcium are considered abnormal due to their increase in resistance with pressure. It is primarily this property, together with the positive temperature coefficient of resistance and a geometrical mode-of-compression factor, which account for the large dynamic coefficient of resistance observed in shock work with calcium and lithium. Similar results would be expected for piezoresistance properties of ytterbium, strontium, and bismuth.

most promising substrate. Because of the surface roughness of Lucalox it has been difficult to achieve continuous films. Successful deposition on this type of substance has been a goal of the work.

The principal reason for using a metallic oxide such as Lucalox for the substrate is to obtain long-duration recording with minimal signal distortion. It is a current practice in field measurements to decrease the perturbations in and around stress gages placed in rocks and soils by using impedance-matching grouts. While impedance matching does decrease the magnitude of the perturbations, it is practically impossible to eliminate them, and stress and mass velocity equilibrium takes place between the transducer and soil by a series of three-dimensional wave reflections in the transducer. These wave reflections are a source of unwanted signals, particularly in the metallic piezoresistance gage, which is sensitive to transverse mass velocity (as distinguished from mass flow along the gage axis). If sufficiently severe, the transverse flow can cause failure of the gage.

By using materials with a low compressibility, high elastic yield stress, and high modulus (compared to that of the soil) such as Lucalox, as a medium directly surrounding the piezoresistive element, it may be possible to decrease the magnitude of the lateral displacement of the sensitive element, since the mass velocity will be less at a given pressure than that of the soils or soil matching epoxies. Axial mass flow equilibrium, required for a stress measurement can be maintained by the use of a thin disc of the low compressibility material. The final goal of the present program has been to develop configurations of such materials in soil matching gages adequate to achieve long recording durations.

3. EXPERIMENTAL CONSIDERATIONS

3.1 Piezoresistance Material Selection

The first consideration in selecting materials for initial work is the expected relative stress-resistance sensitivity of the material. An estimate of the dynamic piezoresistive coefficient of a material can be obtained from static piezoresistive and compressibility data. We expect to observe a difference between the pressure coefficient of resistance obtained under static (hydrodynamic) loading and the stress coefficient of resistance obtained under dynamic (shock, uniaxial stress) loading. This difference would be related to several factors, including: (1) geometrical mode of compression, (2) temperature, and (3) lattice defect production due to the rate of loading. The degree to which each contributes to the observed resistance difference depends on the stress range and the physical properties of the material. Selected properties of five piezoresistive materials and related parameters of general interest in the study are listed in Table 3.1.

We expect a difference in resistance of a piezoresistance specimen at a given dynamic stress compared to the same specimen at an equal value of hydrostatic pressure because we are measuring resistance. The resistance is a function of the resistivity and the geometry of the specimen. Under hydrostatic compression, the volume decrease results in a decrease in all dimensions of a specimen. Under uniaxial compression of a thin film or wire of small cross-sectional area compared to its length, the volume decrease results in a change of cross-sectional area only. The final volumes will be essentially equal if the material has a low yield stress, which the piezoresistance materials currently being studied appear to have. Therefore, the shock piezoresistance coefficient should be larger than the static coefficient by a factor that is a function of volume. We can obtain an estimate of the ratio of dynamic-to-static resistance change if we neglect temperature effects on the resistivity, that is, $\rho = \rho_{(p)}$ only. Although the volume ratios are not strictly equal due to shock heating and material shear strength, the difference is typically small for low-yield materials (on the order of 1%, for example bismuth, Table 3.1); therefore, $(V_p/V_o)_D \cong (V_p/V_o)_S$ where V is volume, and

Table 3.1

PHYSICAL PROPERTIES OF SELECTED PIEZORESISTIVE CONDUCTORS

Property	Lithium, Li	Calcium, Ca	Strontium, Sr	Ytterbium, Yb	Bismuth, Bi	Units
Atomic No.	3	20	38	70	83	
Density, ρ	0.534	1.55	2.54	6.97	9.74	gm/cm^3
Resistivity, σ	8.55	3.91	23.0	28	107	$\mu\ \Omega$ cm
Melting Point	179	851	769	824	271	^oC
Boiling Point	1317	1487	1384	1193	1560	^oC at 760 mm
Temp. at Vapor Pressure of 1 torr	723	800(s)	740(s)	655(s)	1021	^oC
Temp. Coeff. of Resistance	4.45	4.16	3.8	1.3	4.0	$X10^{-3}\ \Omega/\Omega^oC$
Pressure Coeff. of Resistance at Pressure (Pkbar)						
Static	0.008(15)* 0.008(30)*	0.015(15)* 0.019(30)*	0.06(15)* 0.08(30)*	0.07(15)* 0.16(30)*	0.022(15)* 0.026(25)*	Ω/Ω kbar
Dynamic	0.0238** (0 to 55)	0.024† (0-30)				Ω/Ω kbar
Transition Pressure			45*	39.5†† (25°C)	25.3 (25°C)	kbar
Relative Volume V_p/V_o at Pressure (P kbar)						
Static	0.928(10)* 0.831(30)*	0.112(10)* 0.861(30)* 0.732(80)	0.925(10)* 0.978(20)*	0.94(10)* 0.86(30)*	0.972(10)* 0.94(25.3)*	
Dynamic	0.806(35)§	0.753(81)§		0.745(62)§	0.94(25.5)§	
Specific Heat, C_p	0.83	0.156	0.07	0.03	0.029	cal/gm^oC

(s) Sublimes.
* After Bridgman.
** Reference 11.
† Reference 10.
†† Reference 14.
§ Compendium of Shock Wave Data, UCRL-50108, Vol. 1, Sec. A-1, Lawrence Radiation Laboratory, University of Calif., Livermore, California.

and subscripts p, o, D, and S refer to initial and final pressure or stress, and dynamic and static compression, respectively.

The ratio of resistance R at pressure p to resistance at zero pressure under hydrostatic compression is

$$(R_p/R_o)_S = (\rho_p/\rho_o)_S \ (\ell_p/\ell_o)_S \ (A_o/A_p)_S \qquad (3.1)$$

$$= (\rho_p/\rho_o)_S \ (V_p/V_o)_S^{-1/3}$$

The equivalent ratio for dynamic compression is

$$(R_p/R_o)_D = (\rho_p/\rho_o)_D \ (V_p/V_o)^{-1} \qquad (3.2)$$

Therefore

$$(R_p/R_o)_D \Big/ (R_p/R_o)_S \approx (V_p/V_o)^{-2/3} \qquad (3.3)$$

which is greater than unity, and we can expect not only a difference between static and dynamic piezoresistive coefficients but a difference in coefficients which increases with material compressibility. Because the shock temperature of a material generally increases with compressibility and resistance generally increases with increaseing temperature, we can also expect a more compressible material to exhibit a larger difference between static and dynamic resistance changes. The trend indicated by the dynamic and static piezoresistive coefficients of lithium and calcium appears to be consistent with this expectation. Although the lithium static coefficient is only half of that of calcium, the dynamic coefficients appear to be equal. Lithium is more compressible than calcium and therefore is expected to exhibit a proportionately larger dynamic coefficient. A similar situation would be expected between strontium and ytterbium, the most pressure sensitive of the materials being considered. Although the pressure coefficients of resistance are nearly equal in the low kilobar range, strontium is more compressible. From this standpoint it would be expected that strontium might be the best candidate for a low-stress, high-sensitivity sensor with ytterbium, bismuth, calcium, and lithium following in desending order.

Defect production (about which little is known in shock work) could cause a difference between static and dynamic resistivity stress functions. In manganin, defect production appears to be a logical choice to explain differences in coefficients obtained in various materials. This will be discussed in Section 5.3.

Additional properties of a possible sensor to be considered are the temperature coefficient of resistance, the specific heat, density and resistivity. These properties become important when the long recording capability of a transducer is considered, since the piezoresistive gages are subjected to joule heating. In Table 3.2 the ratio of temperature increase of the materials to that of lithium is given, followed by the specific temperature increase for joule heating pulse of 3 amp and 1 msec duration and a fixed film area geometry and resistance. Also shown is a fraction F expressing the ratio of stress signal determined from static data to temperature signal due to joule heating expected at the end of 1 msec. The magnitude of this fraction is a measure of the usefulness of the sensor for recording low-level stresses for long periods of time; i.e., the ratio of stress-induced resistance change to temperature-induced resistance change should be high. It can be seen from Table 3.2 that ytterbium is superior to the other candidate materials, bismuth, strontium, and calcium being less suitable, in that order. Lithium appears difficult to use for a sensor with long recording durations because of its low melting point. A reduction in power supplied to a lithium sensor would be required with a corresponding decrease in sensitivity. Although recording systems in which less energy is dissipated in the gage could be used (for example, frequency modulated systems) which would make lithium usable, ytterbium still appears to be the most advantageous.

One final consideration in the choice of sensor materials is the relative difficulty of sample preparation. Any useful piezoresistive element must also possess repeatable stress coefficients from sample to sample. Vapor deposition has been shown to be an adequate method of constructing calcium and lithium sensors, although the chemical activity of both has made storage difficult. The same would be expected with strontium.

Table 3.2

RELATIVE TEMPERATURE INCREASES
OF CANDIDATE SENSOR MATERIALS

Material	Temperature Increase Ratio	Temperature Increase (^{o}C)	"Usefulness" Factor, Stress Signal Divided by Temperature Signal
Yb	0.072	55	0.98
Bi	0.013	10	0.55
Sr	0.065	50	0.31
Ca	0.4	300	0.012
Li	1	770	182^{o}C (melting temp.)

Ytterbium on the other hand, is a very stable rare earth, which is soft enough to be worked into various shapes and is available as distilled, 99+% pure material. Bismuth is also expected to be readily made in film or foil forms. In summary, ytterbium appears to be the first choice and bismuth, second choice for high-sensitivity piezoresistive stress sensors. The work reported in the following sections is primarily concerned with the measurement of the shock piezoresistance response of ytterbium.

All three materials, ytterbium,[14] strontium,[15] and bismuth,[16] exhibit nonlinear pressure resistance response in static compression. In the cases of ytterbium and bismuth, a maximum in resistance is associated with a phase transition, ytterbium at $\sim$ 39.5 kbar, which is apparently not associated with a polymorphic phase transition and bismuth at 26 kbar. The maximums in resistance represent the upper limit to the useful range of each expected in shock studies.

Although static data show that the tree materials exhibit nonlinear pressure-resistance behavior, it is possible that the response may be linear under shock loadingas as is the case with calcium.

Finally, the criterion of monotonic stress-resistance response over the low stress region, which is necessary for data interpretation, is met by all three materials.

3.2 Recording Duration

The ultimate duration of recording of a piezoresistive shock stress transducer is determined by the period during which electrical continuity is maintained between the stress sensitive element and its electrical leads. Discontinuity arises from relative displacement between transducer components. The displacement may be either transverse to the shock propagation direction or parallel depending on the loading geometry. Laboratory experiments are carefully designed to maintain one-dimensional flow. In large-scale field measurements, one-dimensional flow cannot be maintained. Failure due to parallel displacement can be minimized expecially at low stress by using materials of similar shock impedances as transducer components, for example in granite using aluminum leads.

Transverse displacement presents a more serious problem since elongation of the piezoresistive element will result in a large change in resistance unrelatable to the stress normal to the shock front. Transverse displacement will result from the spherical divergence of the stress wave common to field measurements and from mismatches in shock properties between the transducer and the medium in which it is placed. The latter source can be minimized by constructing the transducer from pieces of the test medium if possible. However the boundary introduced by the placement of the gage is more difficult to eliminate. Matching grouts have so far provided the best means of minimizing the source of lateral disturbances. The difficulty of assuring adequate grouting dictates that another approach be investigated, namely that of desensitizing the piezoresistive gage to lateral flow.

Laboratory studies have been conducted on spherically divergent waves in rock and tuff[17] in which a stretch-compensating conductor relatively insensitive to stress is placed in the same plane as the piezoresistive sensor. By using a compensator of approximately equal resistivity to the stress sensor, the compensator signal arising from stretching can be subtracted from that of the stress sensor and a signal proportional to radial stress obtained. For this system to yield creditable data much should be known about the medium in which it is used and the stretching effect must be small compared to the piezoresistive effect in the sensor.

At low stresses, that is below the plastic range, and in relatively incompressible materials like plastic, these conditions are probably met, although changes in the resistivity caused by plastic deformation may contribute to the observed signal. An example of this type of change is discussed in Section 5.3.

Above the elastic limit of the test medium the change in resistance of the sensor due to stretching may become an appreciable percentage of the total signal.

We can estimate the percentage for a typical field test system as follows: The resistance due to stretching of a wire in spherically divergent flow is derived in Appendix A and is given by

$$\log R_s = \frac{2u_p}{r} t + \log r_\sigma \qquad (3.4)$$

where R_s is the instantaneous resistance due to stretching and u_p, r, and t are the particle velocity, radius from the source, and time, respectively, and R_σ is the value of resistance at stress σ. At a radius of 1 m in alluvium, a typical test medium, the particle velocity at 100 kbar is 0.2 cm/μsec and the ratio of stretch induced to stress induced signal after 10 μsec is 1.10. In a manganin piezoresistance gage, the ratio of stress induced resistance to initial resistance is 1.29 at 100 kbar. Therefore the ratio of total resistance observed to initial resistance at the end of 10 μsec is 1.42 or approximately 30% of the observed signal is due to stretching.

Several methods of decreasing sensitivity to stretching follow from the discussion presented above:

(1) Increasing the stress-resistance sensitivity of the piezoresistive conductor, since the change in resistance due to elongation is not a function of this sensitivity (except for possible deformational effects).

(2) Decreasing the lateral displacement at any given stress by encapsulating the sensor in a thin wafer of material that resists the lateral flow in the test medium. Such a material must have high shear and tensile strengths and high moduli. Encapsulating the sensor in such a material must by necessity distort the wave in the test medium since it cannot be in complete equilibrium if the lateral flow is restricted in the thin wafer. However, the difference may be negligible.

(3) Combining methods 1 and 2 with a stretch compensator. Knowledge of the resistance as a function of stress, temperature, and deformation are required of the material used as a compensator.

Investigations of means of accomplishing methods 1 and 2 are reported in the following sections. Ways to combine techniques (method 3) have not been investigated.

4. EXPERIMENTAL TECHNIQUES

4.1 Sample Preparation. Metallic specimens suitable for shock loading were prepared by vapor deposition and by rolling thin foils from bulk samples. Ytterbium, bismuth, and strontium samples were obtained from Research Chemicals.* Manufacturer's nomenclature and ordering information are given in Table 4.1 for the materials used in the present study.

Table 4.1

MANUFACTURER'S NOMENCLATURE FOR SAMPLES

Material	Lot	Form	Purity (%)	Cost/gm
Ytterbium	K5584G	Ingot (distilled grade)	99.9	$0.90
Bismuth	K707B	Rod	99.9999	$0.12
Strontium	K4937	Rod	99+	$0.12

Two configurations of substrate-vapor deposited film samples were used during the course of the investigation, as shown in Figures 4.1 and 4.2, respectively. The first consists of a vapor-deposited film approximately 10,000 Å thick in the form of a four-terminal network on a soda-lime glass substrate.** The sample is constructed by first bonding aluminum electrical leads into the glass substrate with C-7 epoxy.† The epoxy acts as a filler between the glass and aluminum and provides a continuous substrate surface. The substrate is lapped and polished and then cleaned by solvent rinse, ultrasonic cleaning with detergent solution, triple dionized water rinse, and hot vapor degreasing in trichloroethylene.

---

* Research Chemical, Phoenix, Arizona.

** Soda-lime glass, ρ = 2.59 gm/cc.

† Trademark, Armstrong Products, Inc., Warsaw, Indiana.

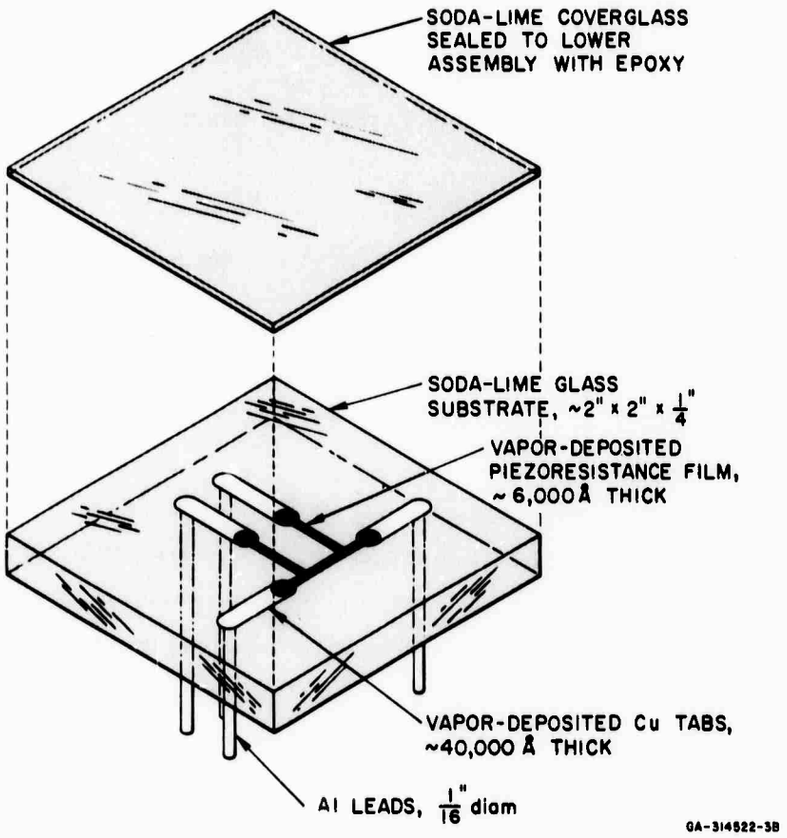

FIGURE 4.1 PIEZORESISTANCE FILM-GLASS ASSEMBLY, CONFIGURATION 1

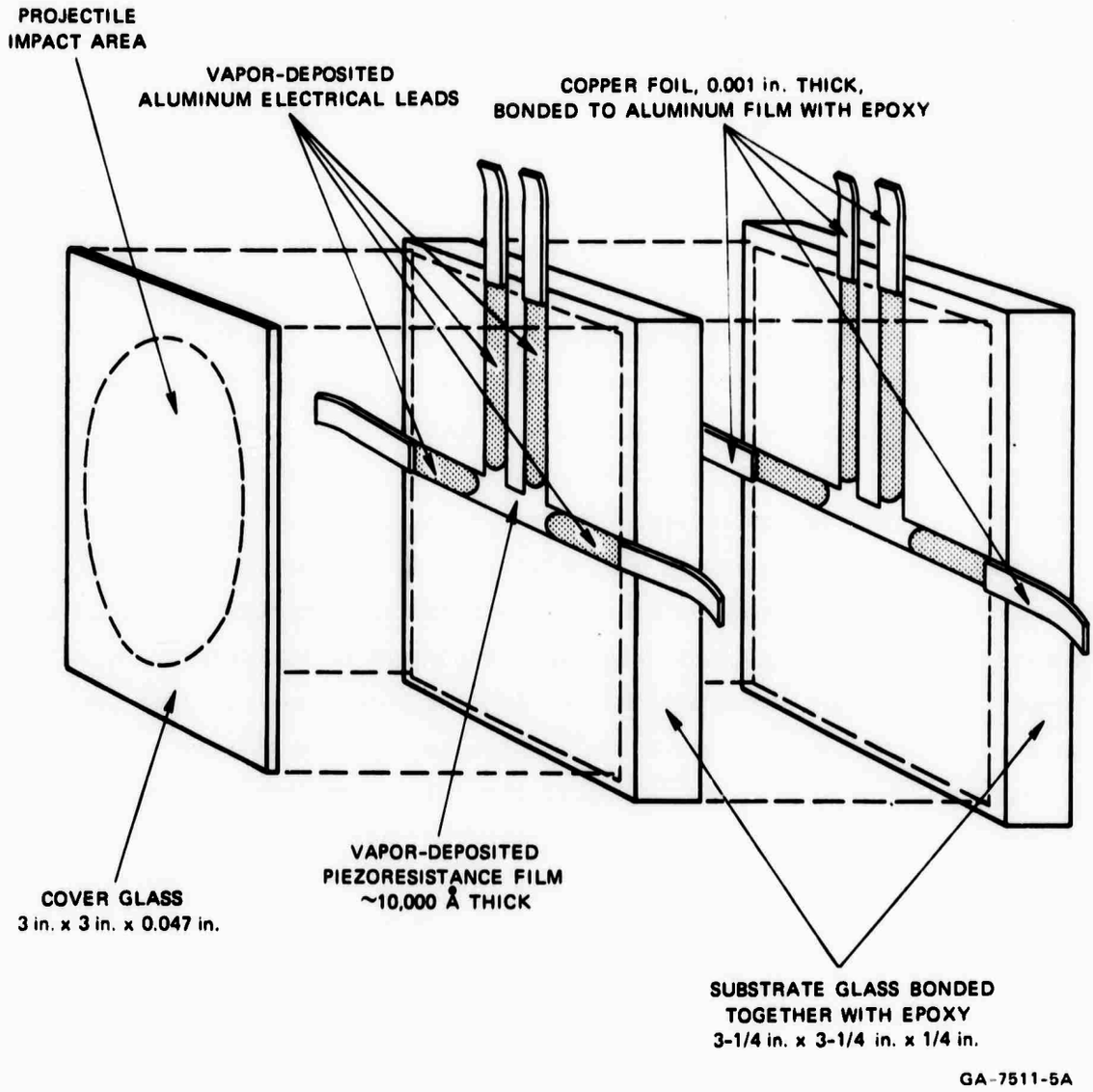

FIGURE 4.2 PIEZORESISTANCE FILM-GLASS TARGET ASSEMBLY FOR THE MEASUREMENT OF RESISTANCE AND GLASS HUGONIOT, CONFIGURATION 2

Clean substrates are required to ensure adequate bonding of the vapor-deposited films.

After cleaning, copper tabs are vapor deposited as shown in Figure 4.1. The tabs were found to be necessary for the bridging from the glass to the aluminum leads across the epoxy filler. When bridging was attempted with the deposited piezoresistive film, it was found that erosion of epoxy occurred which prevented bridging. All depositions were performed in an Ultek TNB vacuum system* at approximately 5×10^{-6} torr. Molybdenum boats were heated by joule heating and the samples by conduction heating from the boats. After removal from the vacuum system, a soda-lime cover glass is sealed to the substrate with C-7 epoxy.

Both the electrical resistance and film thickness are monitored during deposition, the resistance by a double Kelvin bridge** and the thickness by a laboratory-constructed crystal thickness monitor.[18] In addition, films are deposited simultaneously on test substrates for subsequent X-ray diffraction analysis and independent thickness measurements. The second configuration, shown in Figure 4.2, differs from that described above in the method of lead attachment and in deposition environment. In place of aluminum rods, aluminum films, are vapor deposited on the substrate. Connections to these films are made by bonding copper tabs to them under pressure with C-7 epoxy. The bond is sufficiently thin and the area large so that the epoxy resistance is negligible. This configuration allows several gages to be easily placed in series as shown in the figure and permits the stress wave to be measured at two stations. The importance of this type of measurement will be discussed later.

The substrate is shock loaded over an area less than the total area of the substrate, as shown by the dashed circle in Figure 4.2. This type of loading is necessary when the leads lie in one plane (Figure 4.2). Were the entire area loaded, the leads would experience a large shear stress at some point along their length and failure would occur soon after the sensitive area was accelerated. In the configuration shown, the leads experience a particle velocity gradient along their length and continuity can be maintained for periods comparable to the durations achieved with the system shown in Figure 4.1, without the complexity of construction of that type of gage.

---

* Ultek Division, Perkin-Elmer Corporation, Palo Alto, California.

** Cat. No. 1415, W. G. Pye Co. Ltd., Cambridge, England.

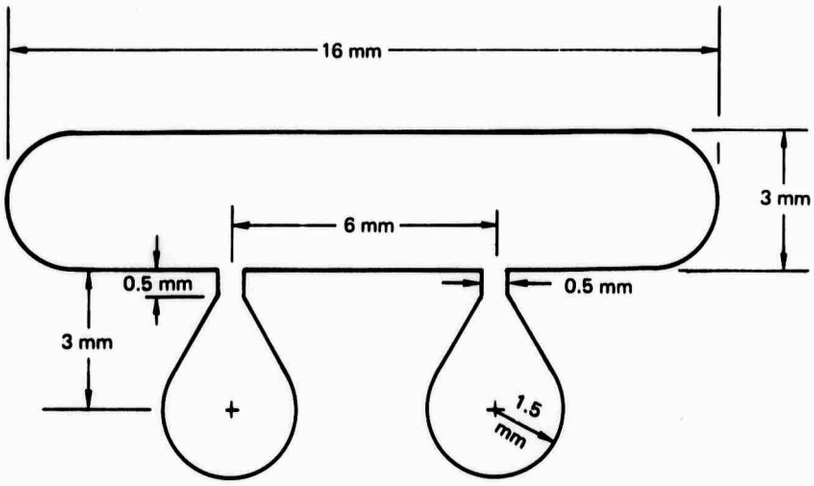

FIGURE 4.3 FOUR-TERMINAL FILM DEPOSITION PATTERN

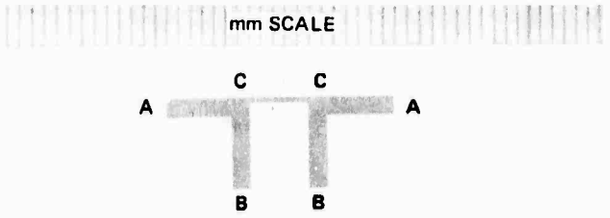

AA) Current Leeds

BB) Voltege or Signal Leeds

CC) Active Portion

GP-7511-10

FIGURE 4.4 YTTERBIUM FOUR-TERMINAL FOIL, 0.013 mm THICK

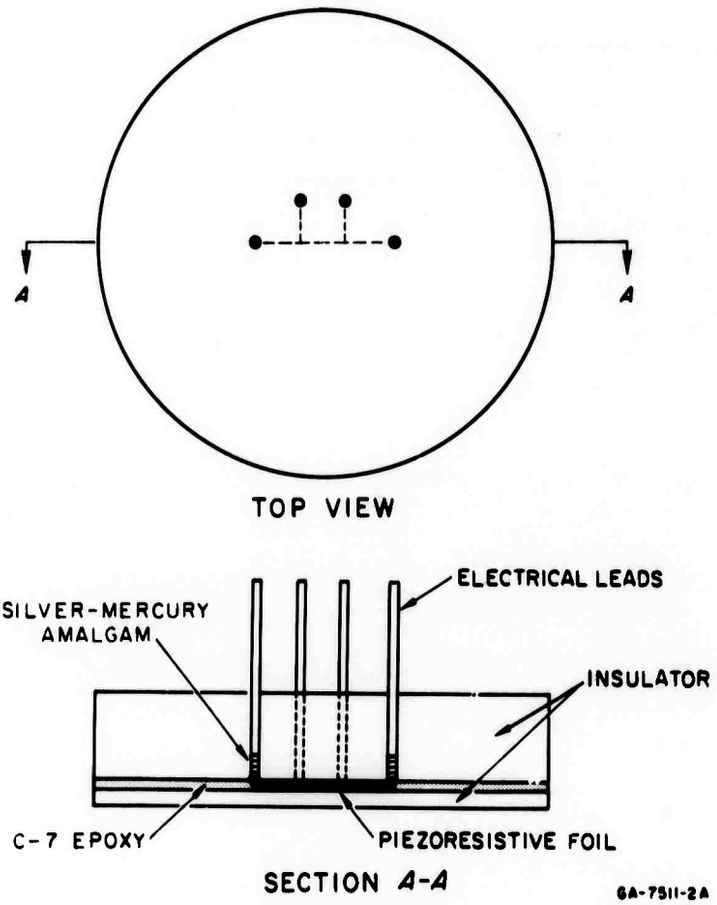

FIGURE 4.5 FOIL-INSULATOR TEST ASSEMBLY

The films of this second type of assembly were deposited in a vacuum system less pure than the first. A standard oil-diffusion pump and fore pump were used instead of the cryogenic and ion pumping of the Ultek system. The reason for the different technique was twofold: (1) more assemblies could be prepared in the diffusion pump system with less time between pumping; and (2) by changing to a less pure environment, the effect of possible contaminents on film resistivity and coefficient could be examined.

The films were deposited through a copper mask to yield the four-terminal (π) pattern shown in Figure 4.3. A small spacer was inserted between the mask and the substrate to electrically isolate the mask from the deposited film.

Foils were prepared by successive rolling of a chip of the bulk sample. Thicknesses of approximately 50,000 Å and larger were obtained in this manner. The thicker films (> 125,000 Å) were free of pin holes, where as the thinner films exhibited a considerable number of holes.

Ytterbium was prepared in both film and foil form, bismuth and strontium in film form only. The foils were constructed into test assemblies by first cutting a π-shaped pattern with sufficient length to the leads to permit electrical contact to be made to them by a conducting filler. A typical foil element is shown in Figure 4.4 and the test assembly in Figure 4.5. Assemblies of this type were constructed from various materials which were chosen because of particular shock properties. Because the shock impedance varied from material to material the electrical leads were also varied to nearly matching properties. In the case of glass specimens, aluminum was used as lead material; for Lucalox, copper leads; for novaculite,* aluminum; and for C-7 epoxy, magnesium rods.

The conducting filler used is dental silver which is mixed with mercury to form an amalgam. The amalgam is packed into the cavity surrounding the electrical lead and the leg of the π-shaped piezoresistive foil.

---

* Homogeneous cryptocrystalline quartz rock.

4.2 Stress-Resistance Measurement. Stress waves were generated by the impact of projectiles upon the substrate assemblies. The projectiles were accelerated to a high, measured velocity by means of gas guns. Both the 1-inch barrel diameter and $2\frac{1}{2}$-inch barrel diameter guns[19] were used in the course of the measurements. A typical arrangement of projectile and target assembly is shown in Figure 4.6. The shock strength in the target is determined by the velocity of the projectile and the shock impedances of the projectile and the target. The calculation of the shock stress can be made for materials with known Hugoniots by either an analytical solution or a graphical solution for the stress-particle velocity state common to both materials. A graphical solution was used in the present work. The method is illustrated in the curves of Figure 4.7. The target Hugoniot is drawn centered about the origin. Interface stress is obtained from the intersection of this Hugoniot and that of the projectile material centered at the projectile velocity.

Aluminum and glass-faced aluminum projectiles were used. The Hugoniot data reported by Fowles[20] was used for the aluminum (2024), and the glass data were obtained from two sources: (1) from Keough and Williams[11] and (2) from a measure of the shock velocity in the case of glass-on-glass impacts. In this symmetrical impact the interface stress is given simply by

$$\sigma = \frac{v\rho_o U_s}{2} \tag{4.1}$$

where v is the projectile velocity, ρ_o is the initial density, and U_s the measured shock velocity. The distances between piezoresistive films (Figure 4.2) was on the order of 6 mm which allows sufficient transit time through the glass (1 μsec) for a measure of shock velocity accurate to ~ 2%. Typical records from this system are shown in Figure 4.8 where R_σ/R_o refers to the ratio of resistance at stress σ to resistance at zero stress.

Analysis of the stress-time data from the several shots indicated that in this stress region, the wave in glass is steady state, since the rise time and peak stress are not a function of travel distance in the glass. At the higher levels (20 kbar) the rise time appeared to be invariant, but the second transducer yielded a lower value of resistance change than the first transducer. This was interpreted as a variation in the piezoresistive

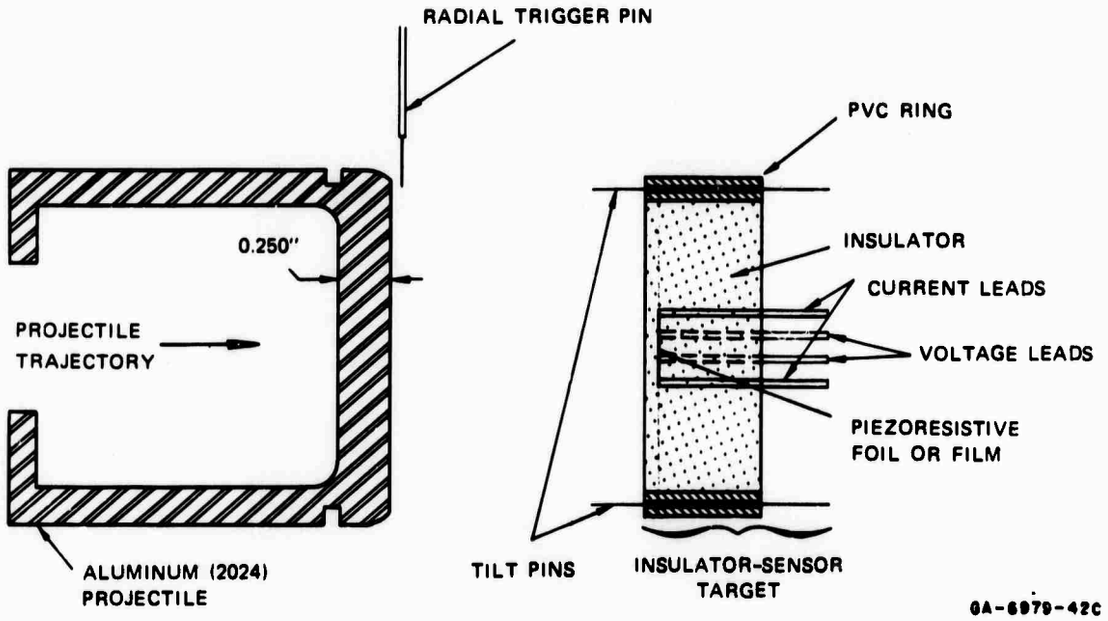

FIGURE 4.6 PROJECTILE-TARGET SYSTEM FOR GENERATING SHOCK STRESS WAVE OF KNOWN CHARACTERISTICS IN PIEZORESISTIVE FOIL OR FILM

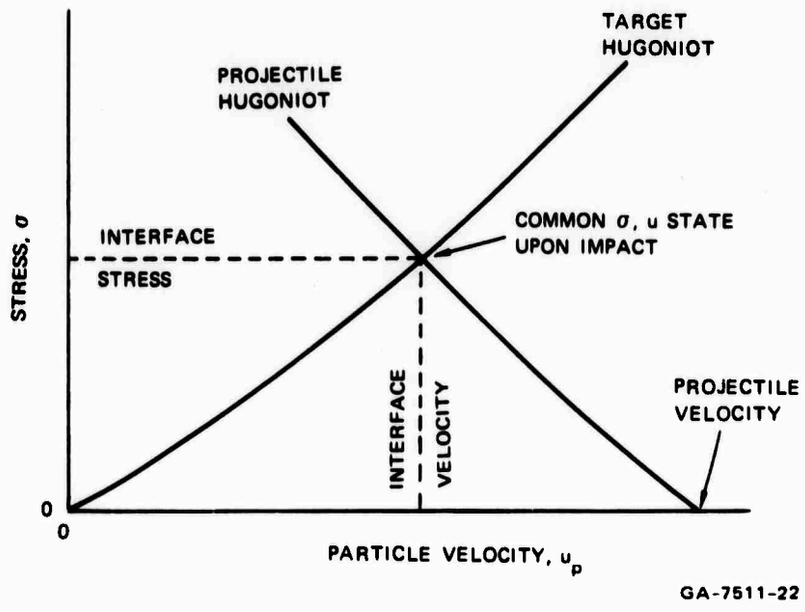

FIGURE 4.7 STRESS-PARTICLE VELOCITY LOCCI OF PROJECTILE-TARGET STATES

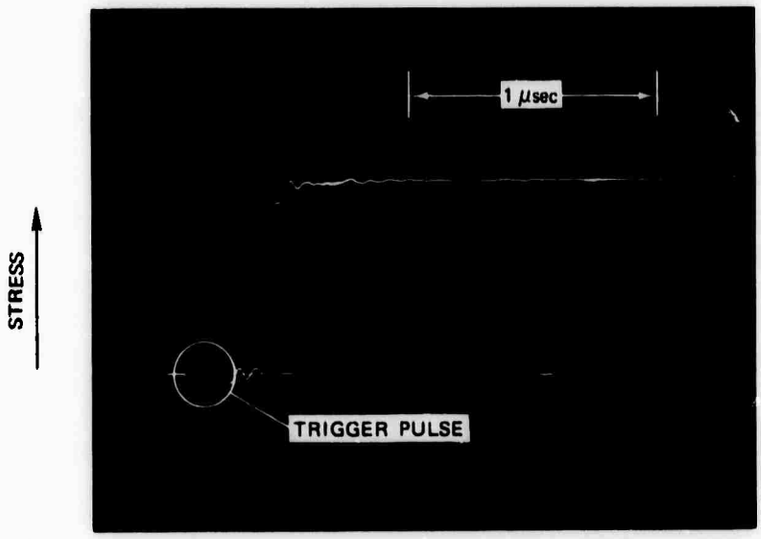

(a) FIRST FILM, PEAK R_σ/R_o = 1.65

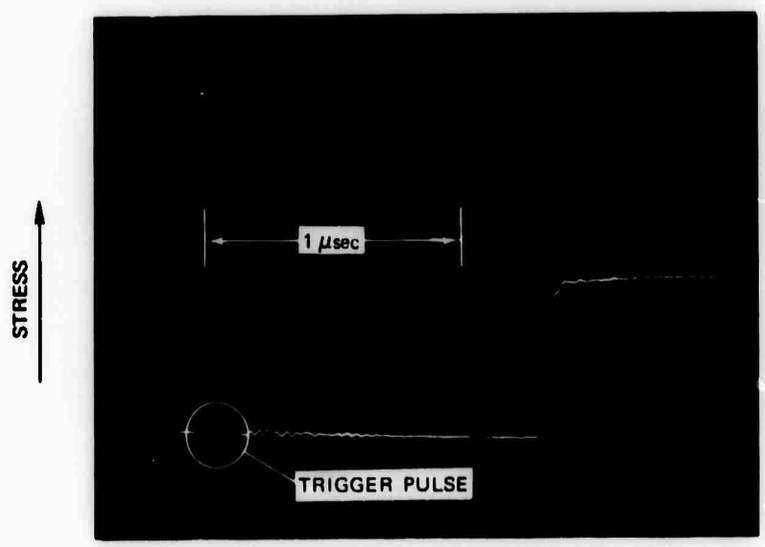

(b) SECOND FILM, PEAK R_σ/R_o = 1.66

GP-7511-6A

FIGURE 4.8 STRESS-TIME RECORDS FROM SUCCESSIVE YTTERBIUM FILMS ON GLASS SUBSTRATES. STRESS = ~ 10 kbar.

coefficient being measured and not as nonsteady shock behavior in the glass. Although some glasses are known to exhibit nonsteady behavior, the invariance of the rise time is not consistent with such behavior. We have therefore interpreted the difference as due to the piezoresistive coefficient.

The stress states in the glass have been calculated assuming steady-state shock behavior as indicated by the invariance of the shock rise with distance. Hugoniot data have been calculated for the glass at each stress state reached. Table 4.2 gives values of density ρ_o, shock velocity U_s, particle velocity u_p, stress σ, and relative volume V/V_o. The Hugoniot data agree very well with previous measurements on similar glass.[11]

The method of generating a series of calculable release stress states is shown in the projectile-target configuration of Figure 4.9 and the stress-particle velocity curves of Figure 4.10. A plate of the higher shock impedance material (Lucalox) thinner than the target material (novaculite) is accelerated to a measured velocity, and upon impacting the target both materials undergo shock compression via waves originating at the interface. The target is made considerably thicker than the impacting plate to assure unloading from the free surface of the latter, as shown in Figure 4.9. Because the shock impedances are mismatched, the impacting plate unloads by a series of stress steps. Correlation of these stress states with the corresponding resistance changes can then be made. A method for the calculation of the stress states is given in Appendix B.

Data for Lucalox were obtained from work by Ahrens, Gust, and Royce.[21] An average value of 10.9 mm/μsec was used for the shock velocity in the region below the Hugoniot elastic limit (HEL). Compression and release data for novaculite were obtained from work by Peterson, Murri, and Cowperthwaite.[22] Their data show that unloading states are essentially the same as the loading states (within 1%, P-V data) in the stress region below 50 kbar. (50 kbar is well below the HEL of novaculite.)

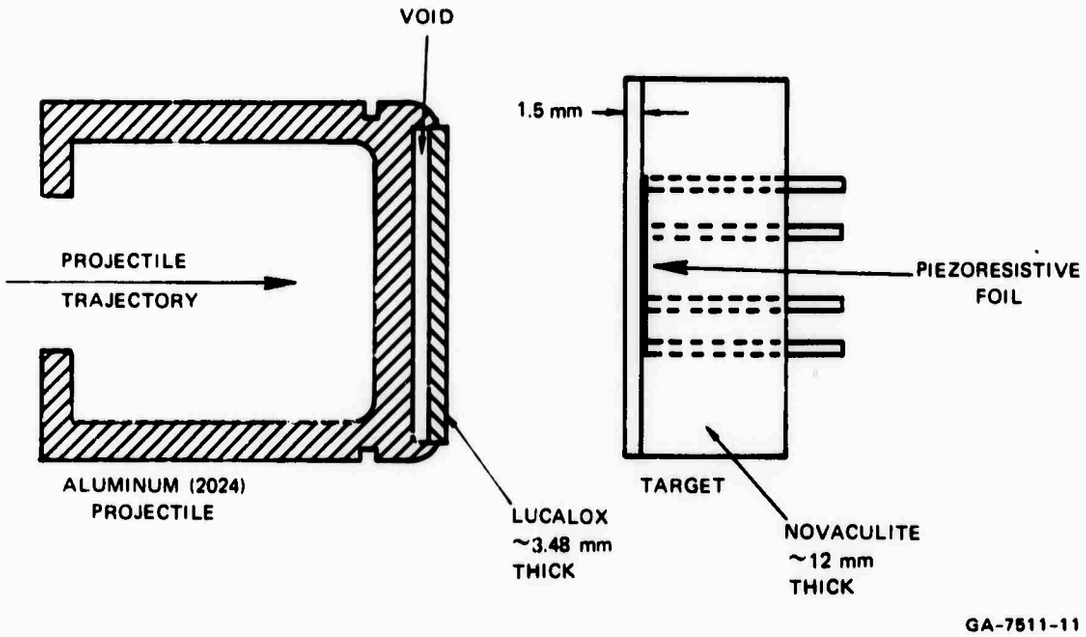

FIGURE 4.9 PROJECTILE-TARGET SYSTEM FOR GENERATING A SERIES OF CALCULABLE RELEASE STRESS STATES

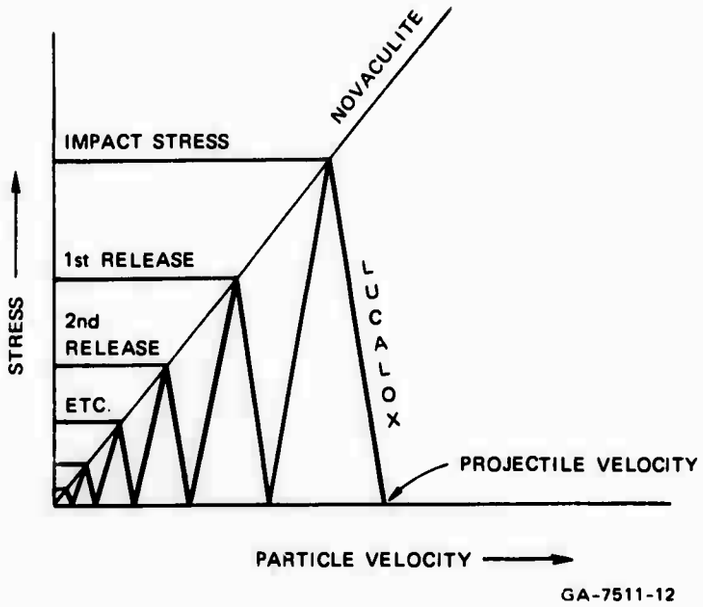

FIGURE 4.10 RELEASE STRESS STATES, IMPACT OF HIGH SHOCK IMPEDANCE MATERIAL (LUCALOX) ON LOWER IMPEDANCE TARGET (NOVACULITE)

Table 4.2

GLASS HUGONIOT DATA

ρ_o gm/cm^3	U_s mm/μsec	u_p mm/μsec	σ kbar	V/V_o
2.49	5.92	0.034	5.0	0.995
2.49	5.92	0.064	9.4	0.989
2.49	5.75	0.134	19.2	0.977

Because of the difficulty of obtaining surfaces suitable for the deposition of films on novaculite, foils were used in the hysteresis measurements. The equivalence of the foil and film response was measured by comparing the compression piezoresistance results of each.

The measurement of resistance of the foils or films as a function of stress and time was accomplished by the use of the electrical system shown in Figure 4.11. The constant-current power supply is turned on a few microseconds prior to shock arrival at the film. By using a constant-current system and a single length of straight conducting film, the effects of contact resistance, film inductance, and capacitance changes under shock loading are minimized. Upon arrival of the shock at the film, the entire film changes resistance. Since the current is constant, the turn on of the power supply results in a voltage signal across the voltage leads π-shaped film. This signal appears on the first oscilloscope as a voltage step proportional to the initial unshocked resistance of the film. On oscilloscopes 2 and 3, it is substracted out by means of offset preamplifiers (Tektronix Type 1A5). This allows the subsequent change in voltage that occurs upon arrival of the shock wave at the film to be recorded at a higher sensitivity. The shock signal appears on the first oscilloscope as an additional step. The percentage increase in resistance is related to the ratio of the two steps. One major advantage of this system is that a voltage calibration is not needed to obtain an accurate measure of the resistance change. In general $\Delta R/R$ is equal to $\Delta V/V$. Cases where the correspondence is not 1 to 1 are discussed in Appendix C.

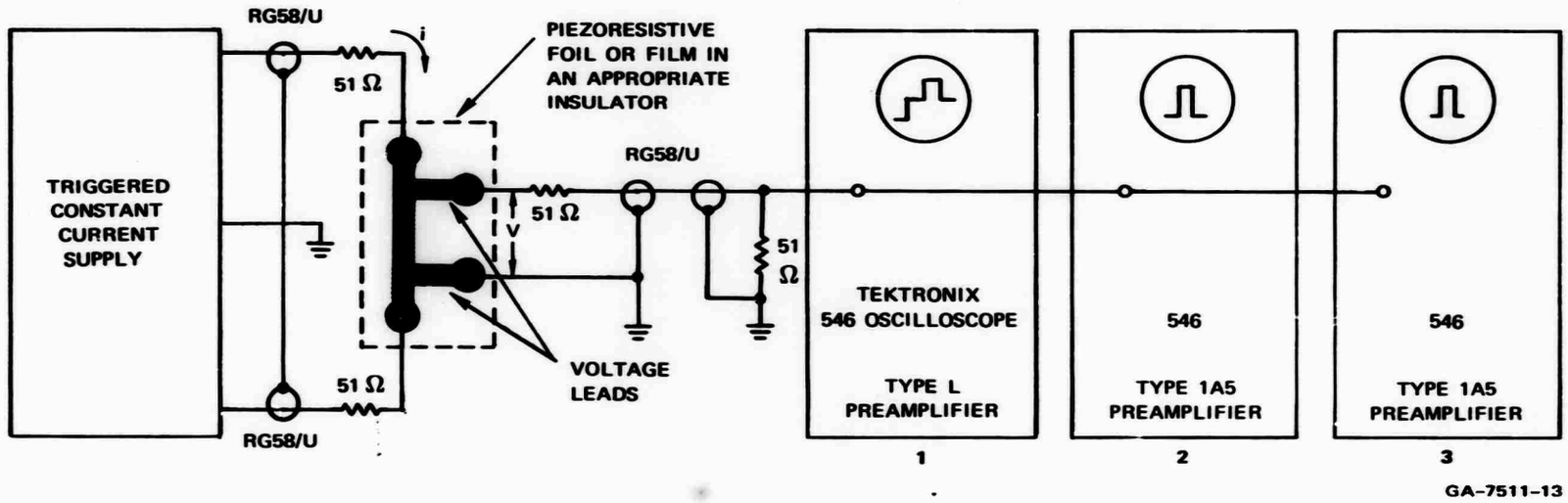

FIGURE 4.11 ELECTRICAL RECORDING SYSTEM

The power supply circuit is shown in Figure 4.12. It has been described previously. However, a description is included here. The power supply is isolated from electrical ground by the capacitor-charging resistors and the trigger transformer T_1. Isolation permits one of the gage signal leads to be grounded, which in turn permits single-ended recording of the stress pulse. The supply is a constant voltage source that produces constant current through the use of a ballast resistance. This resistance is composed of R_6, the crowbar source resistor, and R_7 and R_8 of Figure 4.12. These resistances are distributed to provide a crowbar trigger voltage and power supply cable terminations, respectively.

The operation of the power supply can be best understood by following a sequence of event. When ac power is applied, the charging capacitor C_1 is charged to a voltage limited by the Zener diode string (480 ± 2.4 v). A main trigger voltage derived from delays or from the event to be observed is applied to the main trigger generator, a GE-106-B6 silicon controlled rectifier (SCR). The output from this circuit is transformer-coupled to the gate of the main capacitor discharge SCR (MCR 729-8). The purpose of the trigger circuit is to provide a rapidly rising trigger pulse of constant characteristics regardless of the input pulse to the trigger. The fast turn-on of the main SCR is necessary in situations where there is a short time interval between power supply turn-on and arrival at the piezoresistive film.

The discharge capacitor is shunted with a low-value, high-quality capacitor that permits a rapid current rise in the system. A typical rise time (0 to 100 percent) of the current turn-on is less than 2 μsec. The delay time from external trigger input to current peak is to some extent a function of the rise time of the external trigger. This delay, when the power supply is triggered by the gate of a Tektronix 543B oscilloscope, is on the order of 2 μsec.

Excessive wire heating caused by the dissipation of power in the film is controlled by limiting the duration of the current pulse. The pulse length can be adjusted by using the 20-k potentiometer labeled "Crowbar Adjust" in Figure 4.12. The crowbar is triggered from the current turn-on

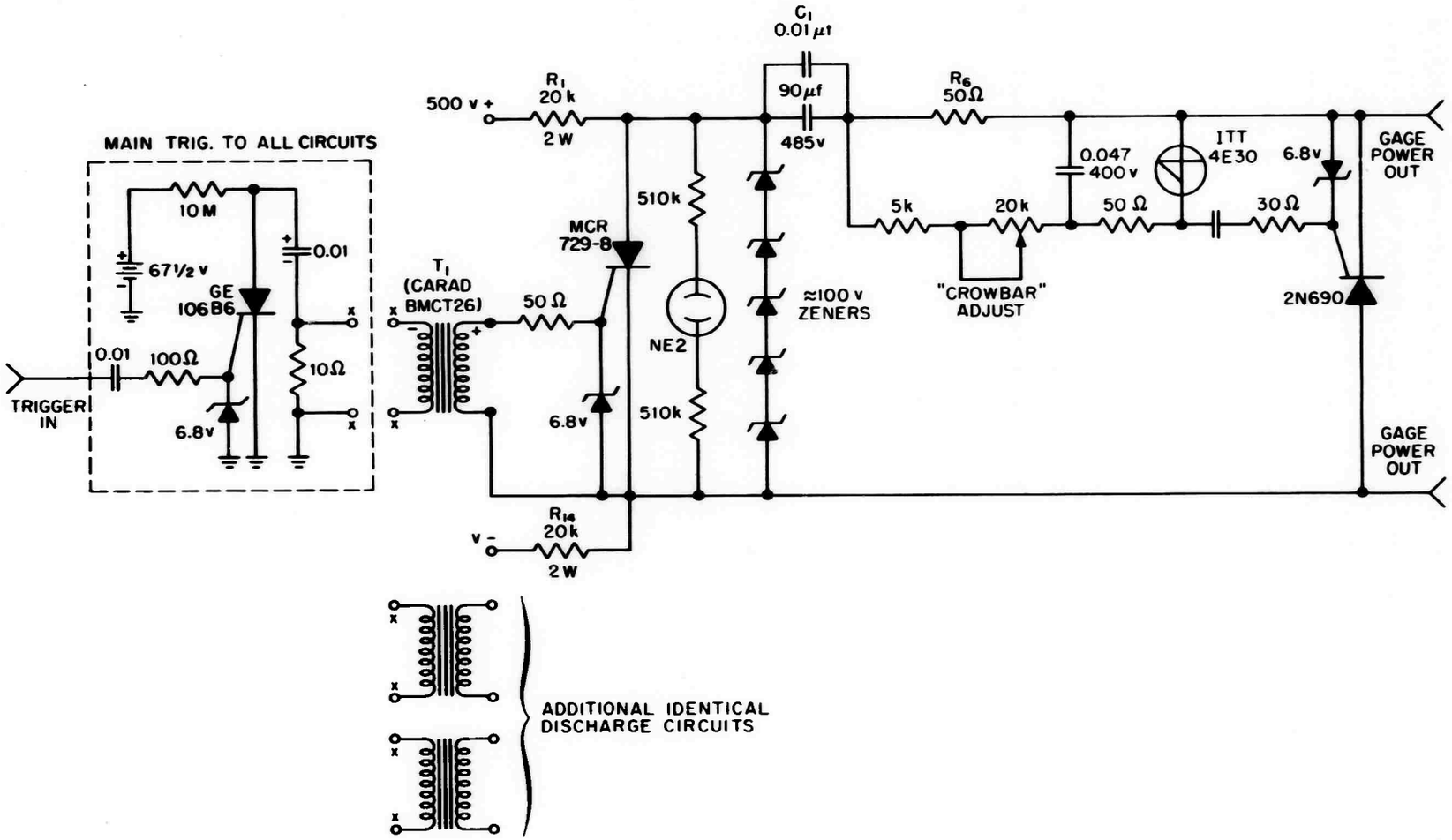

FIGURE 4.12 TRIGGERED CONSTANT-CURRENT POWER SUPPLY WITH DIVERTING (CROWBAR) CIRCUIT

voltage across R_6 delayed by an RC circuit, the potentiometer, and the 0.047-μf capacitor. The delayed voltage triggers the four-layer diode (4E30), which in turn fires the gate of the shunting SCR (2N690). Current is then diverted from the gage circuit to the SCR. With approximately 100-Ω load resistance on the power supply (cable terminations plus gage) and the circuit values shown in Figure 4.12, the crowbar time is adjustable between ≈ 20 and 300 μsec.

Since the voltage on the discharge capacitor is held constant within 0.5 percent by the use of Zener diodes, the voltage across the gage is maintained relatively constant from discharge to discharge. This constancy facilitates oscilloscope input level adjustment prior to an actual shot.

5. RESULTS

5.1 Piezoresistance Materials

During the early part of the program, ytterbium was found to be the most promising of the three materials investigated, ytterbium, bismuth, and strontium. Therefore the major emphasis was placed on sample preparation techniques and piezoresistive measurements on this material and the results reported reflect this emphasis.

5.1.1 Ytterbium

Ytterbium was condensed easily from the vapor phase onto glass substrates. It was necessary to divide the bulk ytterbium into many small pieces to get adequate deposition rates. Since ytterbium sublimes, the increase in area obtainable with the small pieces results in an effectively larger source. No other difficulties were encountered with ytterbium. The films were found to be electrically and chemically stable whether deposited in the cryogenic (Ultek) system or in the diffusion pump system.

Analysis by X-ray diffraction has shown the vapor-deposited yyterbium films to have a lattice constant of 5.48 Å which corresponds to FCC, α-phase ytterbium. This is the phase expected below the transition temperature of 792 ± 5°C at 1 bar. From the film thickness measurements made during deposition and those made after deposition, the film thickness was found to be nominally 0.6 ± 0.1 μ and the resistivity, 37 ± 6 $\mu\,\Omega$ cm. Values of resistivity reported in the literature[23] are lower than this, being 25 to 29 $\mu\,\Omega$ cm; however the limit of error in the present measurement is large due to the uncertainty in the thickness.

The resistance of the deposited ytterbium was measured as a function of temperature while imbedded between glass plates (Figure 4.2). The results are shown in the curve of Figure 5.1. The glass-ytterbium sample was placed in an oven and resistance measured after sufficient elapsed time for thermal equilibrium to take place. A temperature coefficient of $0.6 \pm 0.1 \times 10^{-3}\ \Omega/\Omega\,^{\circ}C$ was measured. This value is approximately 50% of that quoted in the literature (Table 3.1). Possible errors of measurement do not account for the difference. The combined results of

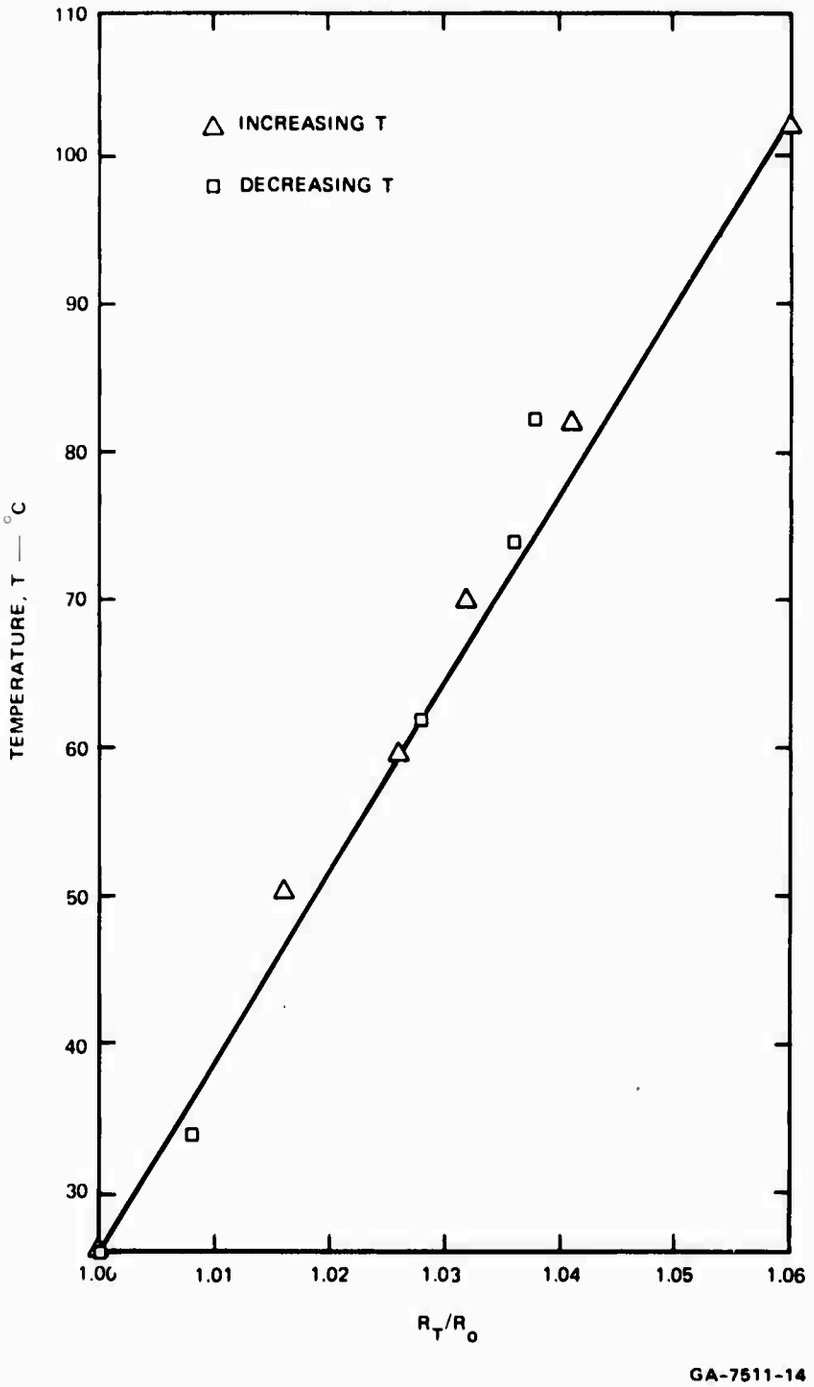

FIGURE 5.1 RELATIVE RESISTANCE OF YTTERBIUM AS A FUNCTION OF TEMPERATURE AT AMBIENT PRESSURE

a lower temperature coefficent and higher resistivity suggest that ytterbium films may have contained some impurities.

Three types of shock measurements were made on the resistance of ytterbium as a function of (1) peak stress, (2) peak stress and temperature, and (3) unloading stress (stress-resistance hysteresis). All data points are shown in the stress-resistance curve of Figure 5.2 and in Table 5.1. The points labeled configuration 1 refer to the substrate system shown in Figure 4.1.

In configuration 1, a correction to the measured values of voltage changed divided by initial voltage was required to obtain $\Delta R/R$, because of the large change in voltage caused by lead resistance which is a function of stress. The data in Table 5.1 include this correction (see Appendix C). In configuration 2, the voltage lead width was increased sufficiently and the resistance decreased so that a correction to these data was not necessary.

In Figure 5.2 is shown one data point labeled 100°C. This point was obtained by preheating the ytterbium with pulsed current (joule heating) prior to shock loading. The temperature was calculated on the basis of assuming no heat loss in the heating interval ($\sim$ 60 μsec) and a substantially constant film resistance. An additional unheated ytterbium film was tested in the same experiment as the heated sample and was shocked to the same stress (11.2 kbar). The data point from the unheated film agrees with the heated film within 1% indicating essentially no temperature effect on the coefficient at this stress.

Hysteresis measurements on ytterbium foils were conducted at $\sim$ 10 and 22 kbar. At both levels, the change in resistance agreed well with that measured for films at the same comparable stress. In fact at the higher level, where stress levels were the same, (21.7 kbar) the agreement was within less than 1%. Relative resistances as a function of unloading stress are shown as the dashed lines of Figure 5.2. In general both curves are displaced from the loading curve in a direction that gives a positive hysteresis. The points at the lower levels below $\sim$ 5 kbar lie on essentially the same curve (within the experimental error).

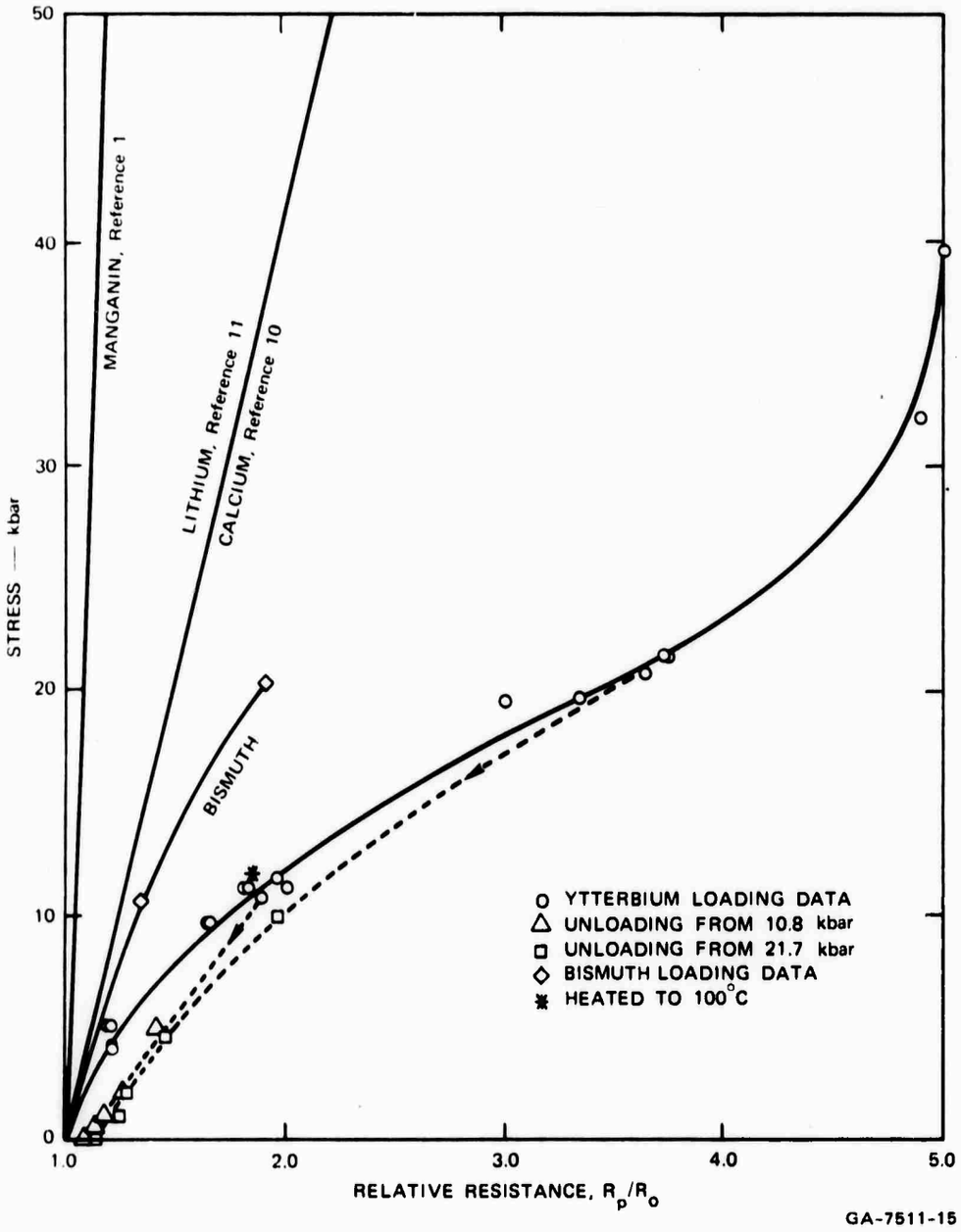

FIGURE 5.2 SHOCK STRESS VERSUS RELATIVE RESISTANCE OF YTTERBIUM, BISMUTH, LITHIUM, CALCIUM, AND MANGANIN

Table 5.1

YTTERBIUM LOADING AND UNLOADING PIEZORESISTANCE DATA

Stress (kbar ± 3%)		Relative Resistance (R_p/R_o ± 2%)			
Loading Peak	Unloading	Raw Data	Corrected	Insulator	Configuration
4.0		1.22	1.22	Glass	1, Film
4.2		1.22	1.22		2, Film
5.0		1.21	1.21		
9.6		1.60	1.65		
		1.64	1.66		
10.8		1.90	1.90	Novaculite	Foil
	5.0	1.42	1.42		
	2.2	1.26	1.26		
	0.9	1.19	1.19		
	0.4	1.14	1.14		
	0	1.11	1.11		
11.2		2.02	2.02	Glass	1, Film
11.2		1.79	1.82		2, Film
		1.80	1.83		
11.6		1.98	1.98		1, Film
19.7		3.12	3.35		2, Film
		2.43	3.01		
20.8		3.33	3.65		1, Film
21.7		3.44	3.76		
21.7		3.75	3.75	Novaculite	Foil
	9.9	1.97	1.97		
	4.6	1.46	1.46		
	2.1	1.27	1.27		
	0.95	1.23	1.23		
	0	1.13	1.13		
32.2		4.35	4.90	Glass	1, Film
39.5[a]		4.45	5.05		

a. Assuming transition at 39.5 kbar, Reference 14.

The residual relative resistance at zero stress agrees to within less than 1% indicating that the residual resistance is not a function of peak stress as is the case in manganin.[1] The unloading response appears to be nonlinear as is the loading curve, although the response from the lower data peak stress can be fitted acceptability well by a linear resistance-stress response.

An interesting, unexplained feature of the stress-resistance waveform was noticed in the hysteresis experiments. A typical record is shown in Figure 5.3. The peak stress is 10 kbar. The unloading stress-resistance response shows a small increase in resistance just prior to the second relief step arrival. The stress at this level is 5 kbar and is well below the stress region (15-5 kbar) of a phase change from FCC to HCP.[24] The character of the signal is very similar to that reported by Wong[25] for a change in magnetic susceptability of iron samples under shock loading. A similar increase in resistance was noted at a higher unloading stress, ~ 10 kbar in the higher pressure experiment. Since both increases occur at the same relative points, i.e., at the end of the first unloading step, it is possible that it is associated with the properties of the impacting plate (Lucalox).

An additional feature of the hysteresis experiments is worth noting. It is illustrated in Figure 5.4 which is a longer time coverage of the record obtained on the 21-kbar hysteresis experiment. As seen in the resistance-time trace, the first compression cycle is followed by an additional cycle, that occurs as the aluminum projectile impacts the Lucalox flyer. A shock is transmitted thru the flyer to the novaculite-ytterbium gage. Although the time resolution is insufficient to measure quantitatively the response of ytterbium and the stress states are not defined, it can be seen that the hysteresis at zero stress is essentially zero, indicating a change in behavior after one stress cycling. Additional experiments of this type were not performed, although it is conceivable that a system could be constructed that would yield quantitative data on successive cycles. Such work might lead to development of a piezoresistive gage with no hysteresis.

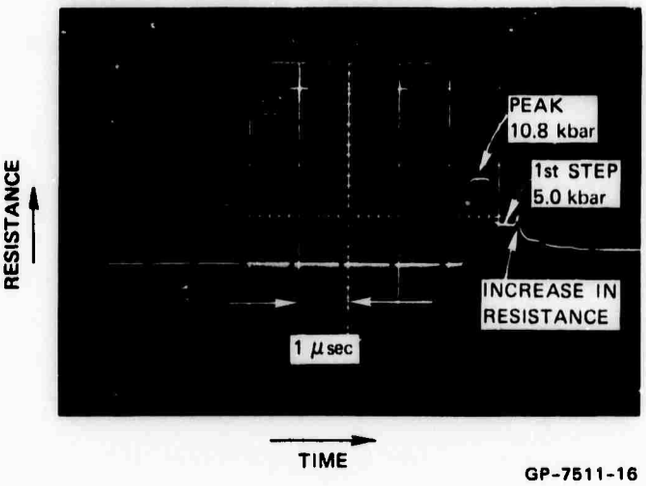

FIGURE 5.3 RESISTANCE-TIME RECORD OF YTTERBIUM IN NOVACULITE, RELEASE STRESS CALIBRATION

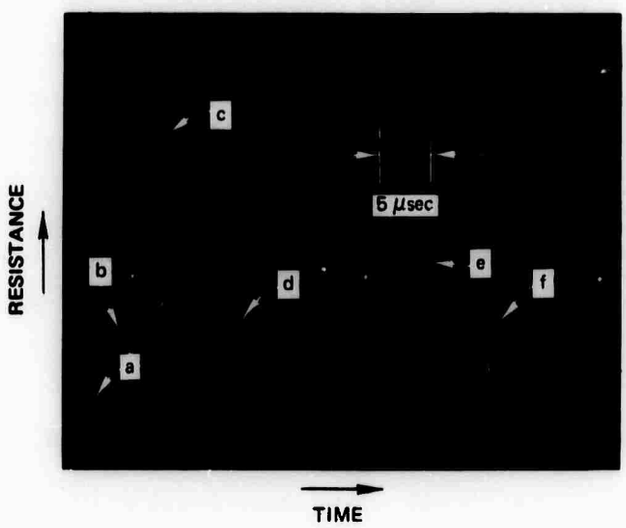

a) Baseline

b) Resistence Prior to Shock

c) Peek Resistence, R_p/R_o = 3.75, Stress = 21.7 kbar

d) Residuel Resistance, R/R_o = 1.13, Stress = 0

e) Peek Resistance, Second Impact

f) Residuel Resistance, R/R_o = 1.0, Stress = 0

GP-7511-17

FIGURE 5.4 RESISTANCE-TIME RECORD, DOUBLE IMPACT EXPERIMENT ILLUSTRATING ESSENTIALLY ZERO HYSTERESIS AFTER STRESS CYCLING

One shock experiment was conducted on ytterbium film in the range of the transition from semiconductor to metallic structure which was designed to bracket the transition. A double-shock system was used in which the first wave raised the stress to approximately 33 kbar and the second to approximately 44 kbar. The resulting stress-time profile showed that the resistance did decrease, as in static work, as the second wave traversed the ytterbium. However, the exaxt transition stress could not be determined. It can be concluded that ytterbium is satisfactory as a high-sensitivity piezoresistive element for use in shock studies below approximately 39 kbar. Although it was difficult to interpret the resistance-time curve of this one shot after the transition (because of the unknown temperature), it is known that the resistance did not drop immediately to that of a metallic conductor as in static work, but rather showed a gradual decrease in resistance during the time interval in which the stress remained constant. It is believed that this is the first evidence in shock studies (other than recovery experiments) of time-dependent or sluggish transitions. If accurate means can be devised to establish shock temperature, the monitoring of resistance as a function of time and comparison with static data may provide a more complete definition of phase transitions.

From our total data compiled to date one can represent the change in resistance R_p/R_o of ytterbium as a function of peak compressive stress σ by

$$\begin{aligned} R_p/R_o &= 1.009 - 6.115 \times 10^{-3}\sigma + 1.157 \times 10^{-2}\sigma^2 \\ &\quad - 3.030 \times 10^{-4}\sigma^3 + 2.011 \times 10^{-6}\sigma^4 \qquad (5.1) \\ 0 < \sigma < &\ 39 \text{ kbar} \end{aligned}$$

with a standard error of $\pm$ 0.105.

5.1.2 Bismuth

Bismuth, like ytterbium, was readily deposited on glass substrates. However, gold tabs were required to bridge the bismuth to the deposited aluminum leads. Bismuth on aluminum resulted in sufficiently high diffusion that lead resistance increased rapidly after deposition.

X-ray diffraction analysis showed the structure of the deposited film to be rhombohedral, which is the crystal structure of bismuth I.

The resistance of bismuth was measured at two stresses, 10.6 and 20.4 kbar. A two-step rise to the resistance was observed at both stress levels. A record of resistance versus stress obtained at 20.4 kbar is shown in Figure 5.5. The projectile configuration was the same as that used for the ytterbium hysteresis measurements, i.e., a Lucalox head 3.48 mm thick mounted on an aluminum projectile as shown in Figure 4.9. The second step corresponds to the time of arrival of the release wave from the rear surface of the Lucalox.

In the lower pressure experiment, 10.6 kbar, a similar step was seen at a time which agrees to within less than 1% of that in the 20.4-kbar experiment. Since the shock velocity in Lucalox is independent of stress in this region, the observed increase in resistance is not thought to be related to an increase in stress but rather is associated with the arrival of the relief wave at the leads and a corresponding change in resistance in the voltage leads. The experiments have been analyzed on the basis of the first increase in resistance. A correction to the raw data was required because of the high lead resistance. Values obtained are given in Table 5.2 and shown graphically in Figure 5.2. A smooth curve has been drawn through the data points and extrapolated to the origin to give an indication of the response compared to the other piezoresistive materials (also shown in the figure). The shock response outside of the two stress ranges shown is not known. However, static pressure data[16] indicate no anomolous effects below the transition stress of ~ 26 kbar.

Table 5.2

BISMUTH LOADING PIEZORESISTANCE DATA

Lucalox Velocity (mm/μsec)	Configuration	Glass Stress (kbar)	R_p/R_o, Obs.	R_p/R_o, Corr.
0.096	2*	10.6	1.309	1.35
0.186	2*	20.4	1.562	1.92

* One gage.

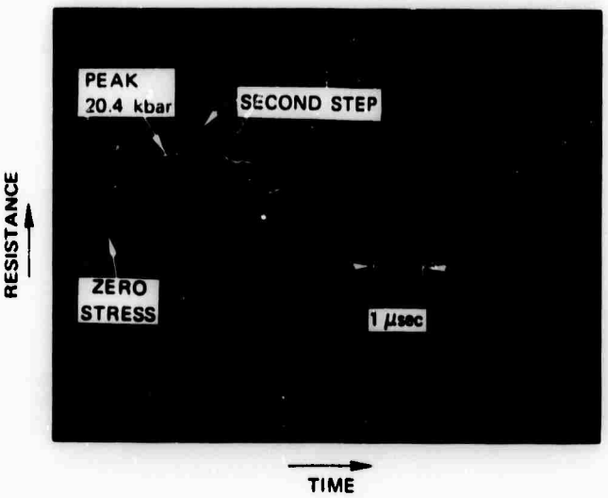

Lucalox Faced Projectile, Velocity = 0.186 mm/μsec
Peak Stress = 20.4 kbar

GP-7511-18

FIGURE 5.5 RESISTANCE-TIME RECORD OF BISMUTH ON GLASS SUBSTRATE, PEAK STRESS CALIBRATION

5.1.3 Strontium

Strontium was vapor deposited on a glass substrate in the Ultek cryogenic vacuum system. A molybdenum boat source was used. However an adequate means of passivating the thin films of strontium was not found. Magnesium fluoride, lithium fluoride, and vapor-deposited paraffin wax were tried. The most successful overlay was magnesium fluoride coated with paraffin wax. The lifetime of this configuration at atmospheric conditions was a few hours. The deterioration of the strontium films was manifested as a change in surface color of the film with a corresponding resistance change. After a few hours exposure, the film resistance and/or the lead resistance increased greatly. Various metals which were not expected to alloy readily with strontium were tried as deposited leads, notably copper and gold. However lead and/or film deterioration was observed with all materials tried. In view of the early successful results on ytterbium no further strontium work was performed.

5.2 Long-Duration Recording

One limitation of a piezoresistive metal-in-epoxy transducer is the sensitivity of the resistance to elongation resulting from nonplane loading and unloading waves, i.e., through three-dimensional mass flow in the epoxy. The sensitivity appears to be a result of the physical elongation of a resistive element as it tends to flow in the epoxy. In the case of an unloading wave originating at the circumference of a circular cross-section gage, sensitivity is manifested as an increase in resistance unrelated to stress.

In contrast to the behavior of manganin in C-7 epoxy, manganin in a more incompressible material, Lucalox, has shown a remarkable insensitivity to the effects of three-dimensional flow. The reason for this behavior is postulated as being related to displacement. Since the particle velocity at equal stress is considerably lower in Lucalox than in C-7 and the modulus much higher, the elongation of the manganin imbedded within should be considerably less for a given time interval.

Experiments with manganin and Lucalox have shown no elongation effects even at stresses as high as 120 kbar. A record illustrating this behavior is shown in Figure 5.6. The aluminum projectile velocity was 0.38 mm/μsec and the peak stress ~45 kbar. The experimental gage configuration was that of Figure 4.5, and consists primarily of a manganin wire or foil bonded between Lucalox discs. Electrical contact between the manganin and external copper posts is achieved via a silver-mercury amalgam filler. The filler is required because voids in the region of transition from the wire in the shock plane to electrical leads normal to the plane result in rapid shearing of the wire and therefore early gage failure during shock loading.

Attempts to achieve long-duration recording in C-7 epoxy by using manganin between thin wafers of Lucalox and the Lucalox imbedded in the epoxy were unsuccessful. Wire elongation occurred at a time equivalent to a typical manganin and C-7 epoxy system of comparable dimensions. Two tests were completed; in the first, copper foil electrical leads were used and in the second, magnesium rods. It was though that the foils sheared upon lateral unloading, however, equal recording durations with each configuration indicate that lead shearing is probably not the mode of failure. The difference in behavior of thick wafers of Lucalox in air, which successfully record for long times, and thin wafers in C-7 epoxy, which do not, is not understood.

In projected actual use of these transducers, the nonplanar flow due to lateral unloading will not be this severe since the shock properties of the gage insulator and surrounding grouting material are matched as closely as possible to the medium in which a measurement is desired (rocks or soils) and the dimensions of the medium are effectively infinite. The perturbations in the plane flow will be much less than in the epoxy-air experiments.

Test configurations were modified to that shown in Figure 5.7 to more closely simulate conditions encountered in field use of these piezoresistance transducers. A grout was chosen* that would closely

* Midi Mist Grout; Hugoniot data and composition obtained from R. Bass, Sandia Corporation, Albuquerque, New Mexico, private communication, 1969.

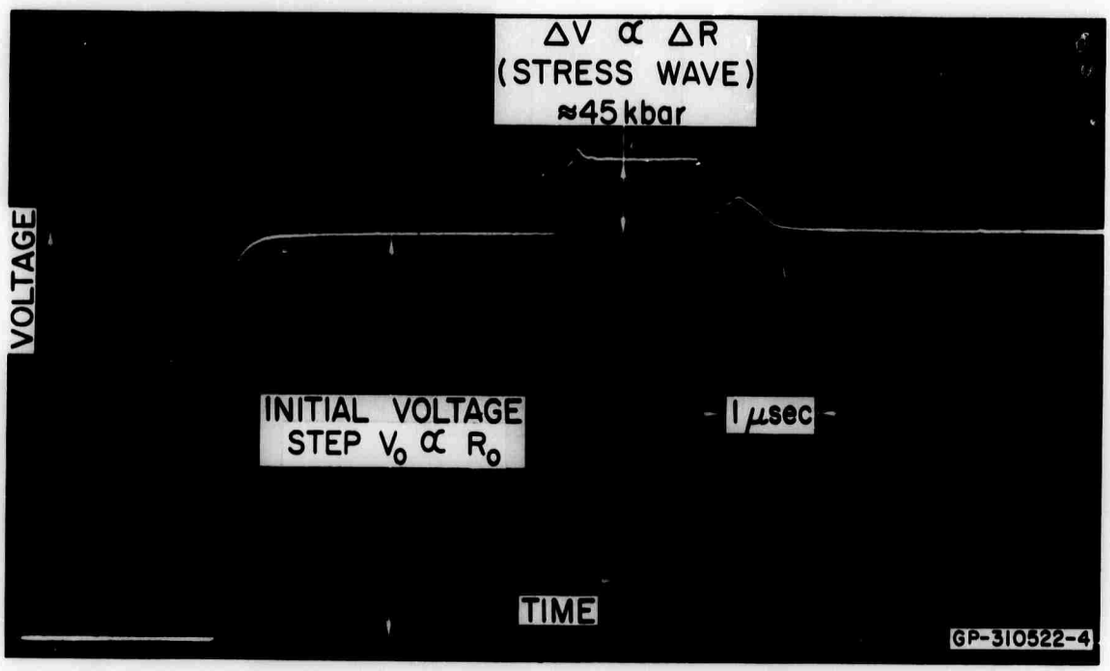

FIGURE 5.6 RESISTANCE-TIME RECORD, MANGANIN FOIL IN LUCALOX IMPACTED BY ALUMINUM FLYER

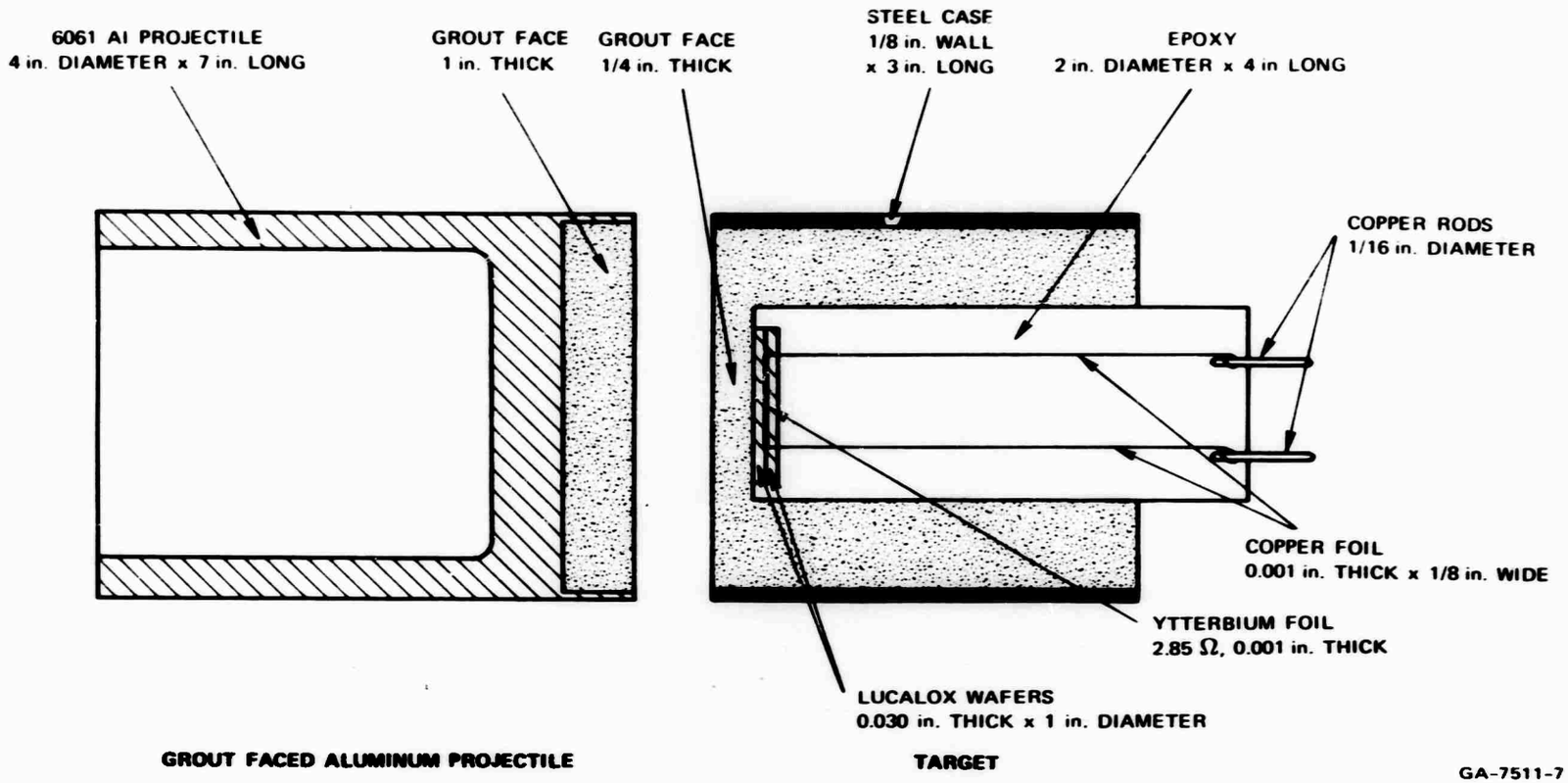

FIGURE 5.7 PROJECTILE AND TRANSDUCER SYSTEM FOR TESTING LONG-RECORDING-DURATION YTTERBIUM-LUCALOX-EPOXY TRANSDUCER

match the shock impedance of the transducer insulator, C-7 epoxy, but not match the shock velocity. With the configuration shown, the mismatched shock velocity allows the shock to lag in the grout that surrounds the test gage. A brief lateral unloading of the test gage occurs which perturbs the plane flow in the gage as might be encountered in an actual field installation. The test gage is similar to those reported above and consists of a 3-Ω ytterbium foil bonded between Lucalox wafers with C-7 epoxy. The Lucalox is quite incompressible and its particle velocity is approximately one-tenth that of the grout or C-7 epoxy at a given stress (in the range of 0 to 10 kbar). The entire grout-gage system is encased in a steel cylinder to delay lateral expansion, i.e., to simulate a semi-infinite medium. One experiment was performed at a gage stress of 3.6 kbar. A grout-faced projectile was used as shown in Figure 5.7. The stress was established from the known Hugoniot of the grout and a measure of the projectile velocity.

The results of the one experiment are shown in the record of Figure 5.8. A precursor wave of 0.4 kbar can be seen, followed by a rise to peak stress, 3.6 kbar, and the arrival of a lateral unloading wave after approximately 10 μsec. A C-7 gage without the Lucalox normally does not indicate a decrease in resistance when unloaded laterally but rather an increase due to elongation of the sensor. Gage failure is seen in Figure 5.8 to occur at ~ 30 μsec. The long duration is attributed to the retardation of lateral flow by the steel cylinder.

5.3 Piezoresistance Response of Manganin

An interesting aspect of the current work with Lucalox and manganin is a possible explanation for a manganin piezoresistive phenomenon noted in earlier work: the apparent sensitivity of the manganin piezoresistive coefficient to the amount of deformation the manganin undergoes. It has been observed that manganin wire exhibits a coefficient in Lucalox which is larger than the $0.29 \pm 0.01 \times 10^{-2}$ Ω/Ω kbar value quoted for manganin in C-7 epoxy.[1] The larger coefficient was noted in the present work for wire geometries. On further examination of past wire Lucalox data, it was found that the larger values occurred only below the Hugoniot elastic

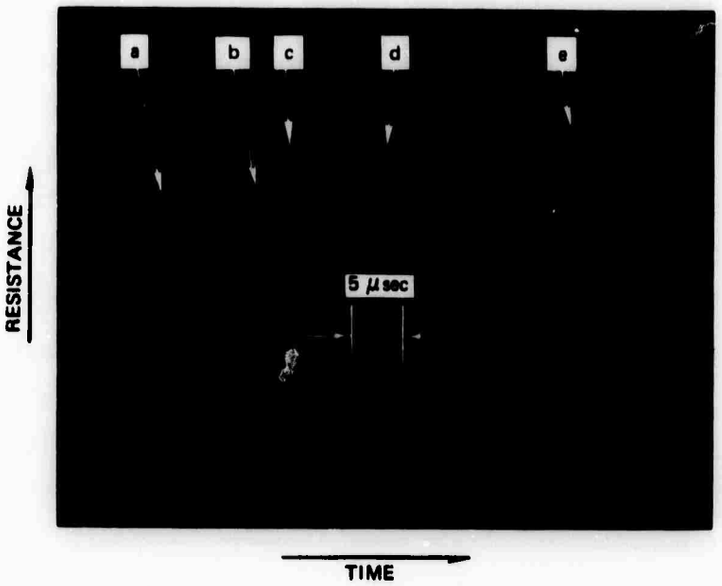

a) Viewing Current Turn-On

b) Precursor Arrival, Stress = 0.4 kbar

c) Shock Arrival, Stress = 3.6 kbar

d) Unloading Wave From Epoxy-Grout Boundary

e) Transducer Failure

GP-7511-8A

FIGURE 5.8 RESISTANCE-TIME RECORD OF YTTERBIUM-LUCALOX-EPOXY TRANSDUCER

limit of the Lucalox. The value in C-7 was again observed above this limit. Below the HEL of Lucalox, the Lucalox can apparently support the shear stress encountered in compressing the wire and hence there is large deformation in the wire with accompanying large defect production. This would result in an increase in resistivity. Calculations of resistivity as a function of stress have yielded values on the order of 5% larger than those obtained with manganin in C-7. The magnitude of this increase is on the order of that observed in deformational tests on cold-worked metals.[26] Confirmation of the cause of the larger observed resistance change of wire gages in Lucalox has been qualitatively obtained by substituting manganin foils ($\sim$ 0.0002 in. thick) for the wire between Lucalox wafers. The high-aspect ratio of the foils, typically 80 to 1, assures that the stress equilibrium process in the foil occurs through a series of one-dimensional wave reflections; i.e., the strain in the foil is substantially uniaxial. The foil results yielded a coefficient in agreement with that obtained with the wire in C-7 epoxy and was considerably less than the wire in Lucalox. Calculated resistivities as a function of measured stress obtained from these tests and prior work with manganin in Hi-D glass, soda-lime glass, Lucalox, and C-7 epoxy are shown in Figure 5.9. The variation in resistivity below approximately 100 kbar for the wire geometry is readily apparent. The corresponding values are shown in tabular form in Table 5.3. Hugoniot data from which calculations of stress resistance and resistivity change were made are shown in Table 5.4 with the source of the data indicated. The resistivity was calculated from:

$$\rho_o = \frac{R_o A_o}{\ell_o} \tag{5.2}$$

where ρ_o, R_o, A_o, and ℓ_o are the initial resistivity, resistance, cross sectional area, and length of the manganin. For both the wire and foil geometries, the length remains constant under shock loading so that the total value change occurs in cross-sectional areas. Thus

$$\frac{\rho}{\rho_o} = \frac{R}{R_o} \cdot \frac{V}{V_o} \tag{5.3}$$

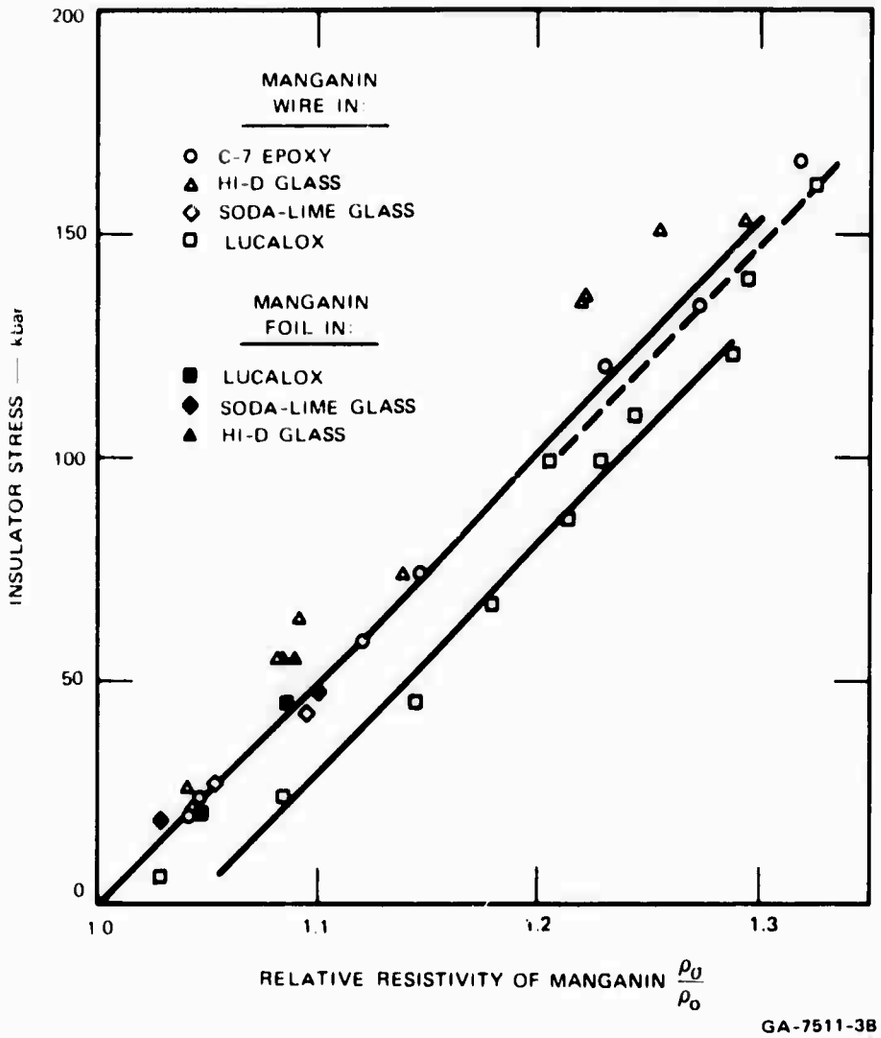

FIGURE 5.9 RELATIVE RESISTIVITY OF MANGANIN FOIL AND WIRE VERSUS INSULATOR STRESS

Table 5.3

HUGONIOT DATA FOR INSULATORS AND MANGANIN

Material	Initial Density (gm/cc)	Shock Stress (kbar)	Shock Velocity (mm/μsec)	Particle Velocity (mm/μsec)	Free Surface Velocity (mm/μsec)	Measurement Technique
C-7 Epoxy[a]	1.18	3.5	-	0.145	-	b,c,d
		8.1	-	0.246	-	
		8.2	-	0.226	-	
		9.4	-	0.281	-	
		15	-	0.426	-	
		15	-	0.409	-	
		23	-	0.550	-	
		28	-	0.645	-	
		38	3.86	-	1.66	e,f
		41	3.97	-	1.74	
		46	4.06	-	1.90	
		51	4.15	-	2.06	
		56	4.24	-	2.20	
		60	4.34	-	2.34	
		65	4.42	-	2.48	
		70	4.51	-	2.62	
		75	4.60	-	2.76	
		81	4.60	-	2.90	
		57	4.38	1.12	-	c,d,e
		74	4.70	-	2.66	e,g

Table 5.3 (Continued)

Material	Initial Density (gm/cc)	Shock Stress (kbar)	Shock Velocity (mm/μsec)	Particle Velocity (mm/μsec)	Free Surface Velocity (mm/μsec)	Measurement Technique
C-7 Epoxy[a]	1.18	74	4.70	1.33	-	c,e,h
		145	5.76	2.14	-	c,d,e
		170	6.20	2.34	-	c,e,h
		170	6.20	-	4.68	e,g
		175	6.34	2.39	-	c,e,h
		190	6.34	-	5.14	e,g
		225	6.79	2.88	-	
		237	6.79	-	5.98	
		259	6.46	-	6.18	g,i
		275	7.19	-	6.48	
		293	8.06	-	6.78	
		368	7.88	3.98	-	c,d,i
		370	7.88	-	7.96	g,i
Soda-Lime Glass	2.52	21.2	5.88	0.144	-	b,c,j
		27.2	5.83	0.184	-	
		43.3	5.94	0.290	-	
Hi-D Glass[k]	6.20	15.4	3.28	-	0.152	e,f
		16.8	3.30	-	0.164	
		17.4	3.31	-	0.170	
		17.8	3.32	-	0.172	

Table 5.3 (Continued)

Material	Initial Density (gm/cc)	Shock Stress (kbar)	Shock Velocity (mm/μsec)	Particle Velocity (mm/μsec)	Free Surface Velocity (mm/μsec)	Measurement Technique
Hi-D Glass[k]	6.20	19.1	3.333	-	0.184	
		20.7	3.34	-	0.200	
		21.3	3.35	-	0.204	
		23.1	3.36	-	0.222	
		24.4	3.36	-	0.234	
		25.2	3.37	-	0.240	
		27.7	3.39	-	0.264	
		29.8	3.39	-	0.284	
		30.5	3.40	-	0.290	
		32.2	3.40	-	0.306	
		33.8	3.41	-	0.320	
		34.3	3.41	-	0.324	
		35.9		-	0.338	
		36.3		-	0.344	
		37.2		-	0.352	
		37.5		-	0.354	
		37.9		-	0.358	
		38.8		-	0.366	
		39.8		-	0.376	
		40.4	3.42	-	0.380	
		37.2	3.40	-	0.352	e, f

Table 5.3 (Continued)

Material	Initial Density (gm/cc)	Shock Stress (kbar)	Shock Velocity (mm/μsec)	Particle Velocity (mm/μsec)	Free Surface Velocity (mm/μsec)	Measurement Technique
Hi-D Glass[k]	6.20	38.0		-	0.364	
		38.8		-	0.368	
		39.3		-	0.372	
		39.7		-	0.376	
		40.1		-	0.380	
		40.5		-	0.384	
		42.6		-	0.404	
		44.5		-	0.422	
		45.0		-	0.426	
		123	3.35	-	1.18	e,d,g
		126	3.39	-	1.20	
		167	3.28	-	1.64	
		221	3.63	-	1.96	

Table 5.3 (Concluded)

Material	Initial Density (gm/cc)	Shock Stress (kbar ± 3%)	Shock Velocity (mm/μsec)	Particle Velocity (mm/μsec)	Free Surface Velocity (mm/μsec)	Relative Volume (V/V_o)	Measurement Technique
Manganin	8.46	56	4.02	-	0.330	0.959	d,e,g
		107	4.36	0.294	-	0.933	c,d,e
		157	4.52	-	0.826	0.909	d,e,g
		254	4.88	-	1.22	0.874	
		346	5.15	-	1.56	0.850	
		360	5.18	-	1.64	0.841	

a. Armstrong Products, Inc., Warsaw, Indiana.
b. Gas Gun.
c. Impedance match, Reference 27.
d. Aluminum driver, Reference 20.
e. In-contact explosive.
f. Two-dimensional wedge, free-surface velocity, Reference 27.
g. Free-surface velocity, inclined mirror, Reference 27.
h. Magnesium driver, Reference 1.
i. Explosively driven flying plate, Reference 20.
j. Shock velocity measured by two manganin gages, Reference 28
k. Penburthy Instruments Co., Seattle, Washington.

Table 5.4

MANGANIN WIRE AND FOIL PIEZORESISTIVITY DATA

Insulator and Manganin Form	Shock Stress (kbar ± 3%)	Manganin Volume Change (%)	Resistance Change (%)	Shock Piezoresistance Coefficient (x 10^3 Ω/Ω kbar ± 5%)	Relative Resistivity	Stress Meas. Technique
C-7 Epoxy Wire	20	1.6	6.0[a]	0.30	1.043	b,c
	24	1.8	6.8	0.26	1.049	b,c
	59	4.2	16.9	0.28	1.120	c,d,e
	74	5.0	20.6	0.28	1.146	
	120	7.4	32.9	0.27	1.231	
	134	8.1	38.6	0.29	1.274	
	166	9.4	47.0	0.28	1.332	
Hi-D Glass (C-7 Bond) Wire	26	2.0	6.3[f]	0.24	1.042	b,c
	55	4.0	12.7	0.23	1.082	
	64	4.5	14.3	0.23	1.092	
	74	5.0	20.0	0.27	1.140	c,d,e
	135	8.1	32.9	0.24	1.221	
	136	8.2	33.1	0.24	1.222	
	151	8.8	37.7	0.25	1.256	
	153	8.9	41.0	0.27	1.285	
Foil	55	4.0	12.9	0.23	1.084	b,c
	55	4.0	12.2	0.22	1.077	

Table 5.4 (Concluded)

Insulator and Manganin Form	Shock Stress (kbar ± 3%)	Manganin Volume Change (%)	Resistance Change (%)	Shock Piezo-resistance Coefficient (x 10^3 Ω/Ω kbar ± 5%)	Relative Resistivity	Stress Meas. Technique
Lucalox (C-7 Bond) Wire	6	0.4	3.4	0.57	1.030	b,c
	24	1.8	10.4	0.44	1.084	
	45	3.3	18.3	0.41	1.144	
	67	4.6	23.6	0.36	1.179	
	86	5.7	28.8	0.33	1.215	
	99	6.4	28.8	0.29	1.206	
	99	6.4	31.3	0.31	1.229	
	109	6.9	33.7	0.31	1.235	c,d,e
	123	7.6	39.4	0.32	1.288	
	140	8.4	41.4	0.30	1.295	
	161	9.2	46.2	0.29	1.328	
Foil	24	1.8	6.5	0.27	1.046	b,c
	45	3.3	12.3	0.27	1.086	
Soda-lime Glass (C-7 Bond) Wire	21	1.6	6.1[f]	0.28	1.044	b,c
	27	2.1	7.7	0.28	1.054	
	43	3.2	13.0	0.30	1.094	
Foil	21	1.6	4.8	0.23	1.031	b,c
	48	3.6	14.1	0.29	1.100	

a. Reference 1.
b. Gas Gun
c. Impedance Match
d. In-contact explosive.
e. Aluminum driver.
f. Reference 11.

BLANK PAGE

6. CONCLUSIONS

6.1 Piezoresistance Materials

It is interesting to compare the piezoresistance response of shock-loaded ytterbium and bismuth with previous, similar work on lithium calcium and manganin and also to compare results with static pressure data.

In comparison with shock work on lithium[11] and calcium[10] (shown in Figure 5.2 and Table 6.1) ytterbium shows a nonlinear response. In the very low stress region, below 1 kbar, lithium and ytterbium show roughly the same sensitivity, if we can extend our measured response of ytterbium at the 4-kbar region to the subkilobar region by means of a least-squares fit to the data. Additional data are needed in the subkilobar region to establish the very low-pressure response. Bismuth, lithium, calcium, and ytterbium in descending order of sensitivity are all approximately 1 order of magnitude more sensitive than manganin (0.29×10^{-2} Ω/Ω kbar) in the subkilobar range.

At 5 and 10 kbar, ytterbium is the most sensitive of these materials, being approximately 14 and 27 times, respectively, as sensitive as manganin and 1.2 to 2.0 times as sensitive as bismuth.

In comparison with static piezoresistance data, ytterbium and bismuth show qualitatively similar response to that expected and as outlined in Section 3.1 above; i.e., the effect of a higher compressibility is to increase the pressure-resistance coefficient. Ytterbium is considerably more compressible than bismuth and shows a correspondingly greater increase in coefficient over static data. The effect of temperature on the coefficient also agrees qualitatively with that found for lithium.[11] If an adjustment is made to the static data (for compressive volume change, see Section 3) a response curve slightly displaced to the right would be obtained at all stress levels (Figure 6.1). However, Hall[14] has reported that at pressures above approximately 10 kbar, $(\partial \ell nR/\partial T)_p$ is negative, the magnitude increasing with pressure. The negative temperature coefficient is characteristic of a semiconductor, which ytterbium is postulated to be at the higher stresses. The net effect of the negative

Table 6.1

COMPARISON OF STATIC AND DYNAMIC PIEZORESISTANCE DATA FOR LITHIUM, CALCIUM, YTTERBIUM, AND BISMUTH

	Static			Dynamic	
Material	Pressure (kbar)	R_p/R_o	V_p/V_o	Stress (kbar)	R_p/R_o
Li	10[a]	1.073	0.926	1.0[b]	1.024
	20	1.152	0.875	10.6[c]	1.235
	30	1.239	0.836	12.5	1.295
	40	1.305	0.799	17.5	1.440
	50	1.366	0.763	23.0	1.550
	60	1.428	0.728	23.5	1.535
				29.5	1.740
				34.6	1.834
				54.5	2.290
Ca	10[a]	1.107	0.942	1.0[d]	1.023
	20	1.258	0.878	18[e]	1.42
Yb	5[f]	1.2[g]	0.97[g]	1.0[h]	1.018
	10	1.5	0.94	4.0[i]	1.22
	20	3.0	0.89	4.2	1.22
				5.0	1.21
					1.22
	30	5.9	0.86	9.6	1.65
					1.66
				10.8	1.90
	35	7.0	0.84	11.2	1.83
	39.5	7.5	0.83		1.82
				11.2	2.02
				11.6	1.98
				19.7	3.35
					3.01
				20.8	3.65
				21.7	3.76
				21.7	3.75
				32.2	4.90
				39.5	5.05
Bi	10[a]	1.210	0.972	1.0[j]	1.033
	20	1.474	0.948	10.6	1.35
				20.4	1.92

a. P. W. Bridgman, Proc. Am. Acad. Arts Sci. 81, 167-251 (1952).
b. Calculated from average coefficient 0.024 Ω/Ω kbar.
c. Reference 11.
d. Calculated from 18-kbar data.
e. Reference 10.
f. Reference 14.
g. Read from graphs of Reference 14.
h. Calculation from least-squares fit.
i. Present work.
j. Calculated from 10.6-kbar data.

temperature coefficient in shock loading would be to decrease the expected magnitude of the change in resistance because of shock heating. Although shock temperature calculations cannot be made at this time because of insufficient data, rough estimates of temperature, combined with Hall's static temperature coefficient results, indicate that dynamic R_p/R_o values would be less than static at higher stresses. This effect is indeed observed as indicated by the "calculated" value shown in Figure 6.1 at 33.5 kbar. Our shock results agree qualitatively with the results expected from statically observed behavior of ytterbium, i.e., the coefficient is larger at the lower stresses where the shock temperature is low and where the temperature coefficient is positive. At the higher stresses, the coefficient is less than the static value.

Quantitatively, the results do not correlate very well with Hall's data. If one assigns the total difference between adjusted static data and observed dynamic data to temperature, the results are not consistent; i.e., larger temperatures are obtained at 10 kbar than at 20 kbar. The quantitative discrepancy may be due to a difference in sample purity which has been shown in static work[14] to have a substantial effect on the observed coefficient.

The repeatability of R_p/R_o at a given stress is somewhat paradoxical. At two stresses, 10.8 and 21.7 foil and film data were identical within the limits of measurement. However, repeated measurements at 11 kbar on films gave a rather large scatter in the data. This might be attributed to the rather large correction for lead resistance required in these data. Additional, more controlled experiments are required, possibly with a 50-Ω grid configuration, in which lead resistance does not enter into the measurement.

The dynamic coefficient of bismuth is larger than the static coefficient by a factor of approximately 1.66 at 10 kbar and 1.94 at 20 kbar. The increases are also much too large to be attributed to volumetric and temperature effects.

The shock piezoresistance measurements on ytterbium can be summarized as follows:

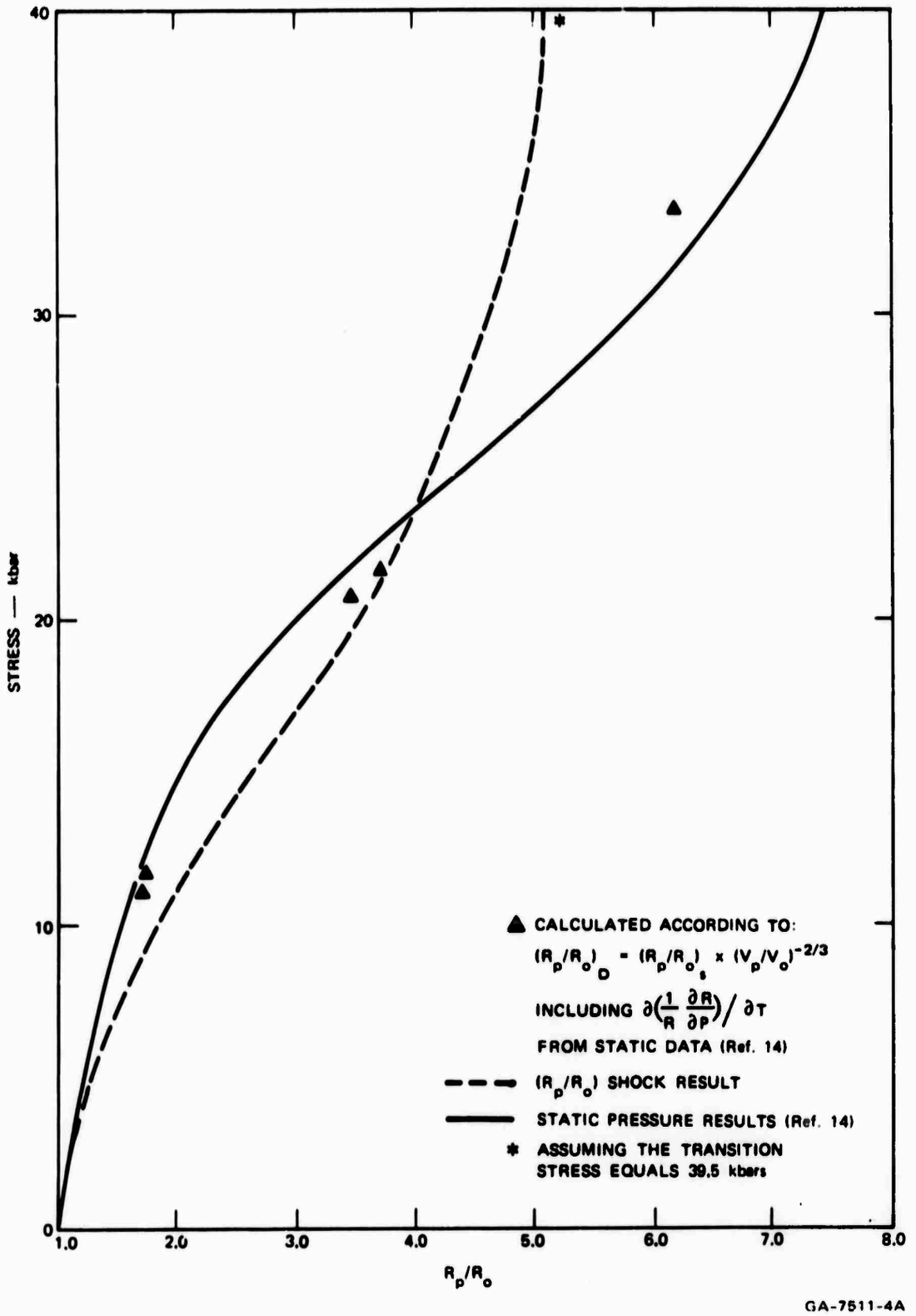

FIGURE 6.1 COMPARISON OF STATIC AND DYNAMIC PIEZORESISTANCE RESPONSE OF YTTERBIUM

(1) The peak-shock stress resistance response of a vapor deposited film is equivalent to that of a cold worked foil. The response is nonlinear, monotonically increasing reaching a maximum at ~ 39 kbar as does the static response. Data are required below 4 kbar to define the subkilobar response. Additional data are also required to establish repeatability.

(2) The vapor-deposited film does not show a temperature dependence of the coefficient at 10 kbar and 100°C, whereas the static coefficient shows a temperature dependence which is slightly negative in this stress range.

(3) The unloading response of foil shows an effectively constant offset (+ 11% and + 13%) when unloaded from 11 and 21 kbar. The unloading response from 11 kbar can be represented by a linear relationship; that from 21 kbar is nonlinear. Both curves are displaced from the loading curve. Within the accuracy of measurement, both curves are monotonically varying functions. In one experiment a second shock showed no hysteresis on unloading.

(4) Qualitatively the loading response agrees with static data. Quantitatively, the temperature effects are too large. Temperature effects also appear to be in conflict with (2) above.

(5) Both foils and films appear to be suitable sensitive piezoresistive sensors for use in shock wave transducers, although the subkilobar response, as yet unmeasured, appears to be about the same as that of lithium, calcium, and bismuth.

(6) A shock-loading/unloading system has been achieved which defines the stress states and hence the stress-resistance hysteresis more accurately than previous systems.

The mechanical work with ytterbium has shown that both foils and films can be readily made, the latter by simple vapor deposition, and both are chemically stable.

Piezoresistance measurements on bismuth indicate that the dynamic coefficient is considerably less than ytterbium in the 5-kbar and up range and roughly equivalent below 5 kbar. Data are needed in the subkilobar range to define the low stress response.

6.2 Long Recording Systems

The concept of decreasing the sensitivity to lateral flow of a piezoresistive stress transducer by encapsulating it in a high-modulus, relatively incompressible insulator and by increasing the piezoresistive coefficient appears to yield long-time recording of the stress in and

around the transducer in a semi-infinite environment. Tests under severely divergent flow, that is, unloading to zero lateral stress from the transducer periphery, showed that the one insulator used, Lucalox, decreased the elongation effect in a large block of Lucalox but did not decrease it when used as a thin wafer. In field test applications, this type of lateral distrubance is not expected. Tests were not performed on spherically divergent flow.

6.3 Manganin Response

One important conclusion that can be drawn from the present investigation is that if manganin is to be employed as a quantitative dynamic stress sensor in a variety of materials, the mode of compression of manganin must be considered carefuliy. It appears from the present results that the most promising configuration for obtaining dynamic, principal stress measurements independent of the stress distribution in the surrounding insulators is a thin foil with a high aspect ratio (e.g., 100:1).

7. RECOMMENDATIONS

In view of its shock piezoresistance behavior and mechanical properties, ytterbium appears to be the most promising sensor of the materials tested for the low kilobar range. Further work on this material in the low and subkilobar stress region is required before its shock response during loading and unloading can be stated with sufficient accuracy and repeatability to be used as a "standard" piezoresistance material. Bismuth, although slightly more difficult to use in film form, may be as adequate as ytterbium in the subkilobar region. Specific areas of future work should include:

(1) Measurements should be made of the compression piezoresistance coefficients of both bismuth and ytterbium from a few kilobars to the subkilobar region.

(2) Additional measurements should be taken of the unloading response of ytterbium over a range of stresses. Similar measurements should be made on bismuth.

(3) Repeatability of resistance-stress response should be examined more closely. Specifically, constituent impurities of deposited films should be determined more accurately than in the present work and possible correlations with repeatability of the coefficient examined.

(4) With respect to long-duration recording of systems embedded in soils and rocks, it is recommended that a few field tests be performed with the present configuration of ytterbium-Lucalox in epoxy. Specifically, small-diameter (~ 2-inch) gages can be placed in alluvium or tuff (reasonable impedance matches to C-7 epoxy) and the response measured in the low-kilobar, few-hundred-microsecond environments. Laboratory experiments should be continued, however, since it is felt that the mechanics of the use of high-modulus, high-impedance insulators is not sufficiently understood to be optimized.

BLANK PAGE

Appendix A

ESTIMATE OF RESISTANCE CHANGE DUE TO WIRE STRETCHING IN SPHERICALLY DIVERGENT FLOW

Consider a wire of cross-sectional area A of dimensions small compared to the length ℓ. Let the wire subtend an angle θ and be a distance r from the center of a spherically divergent source where $r \gg \ell$. The rate of change of resistance for plastic elongation of the wire, assuming constant resistivity and volume, i.e., at a constant stress σ, can be found as a function of particle velocity, radius, and time from:

$$R = \rho \frac{\ell}{A} \tag{A.1}$$

$$dR = \rho \left(\frac{d\ell}{A} - \frac{\ell}{A^2} dA \right) \tag{A-2}$$

and

$$dA = - A \frac{d\ell}{\ell} \tag{A.3}$$

since the area decreases as the length increases. Therefore

$$dR = 2 \rho \frac{d\ell}{A} \tag{A.4}$$

and

$$\frac{1}{R} \frac{dR}{dt} = \frac{2}{\ell} \cdot \frac{d\ell}{dt} \tag{A.5}$$

but

$$\frac{d\ell}{dt} \approx \frac{dr}{dt} \cdot \theta \tag{A.6}$$

if the wire flows with the surrounding material

and

$$\frac{dr}{dt} = u_p \tag{A.7}$$

the radial particle velocity. Therefore

$$\frac{1}{R} \frac{dR}{dt} = \frac{2 u_p}{r} \tag{A.8}$$

where r is the instantaneous radius.

If r is large, then r and u_p are effectively constant for short intervals since $u_p \propto \sigma \propto \frac{1}{r}$ and the resistance at time t is:

$$\int \frac{dR}{R} = \frac{2\,u_p}{r} \int dt \qquad \text{(A.9)}$$

$$\log R = \frac{2\,u_p}{r}\, t + C \qquad \text{(A.10)}$$

$$t = 0,\ R = R_\sigma,\ C = \log R_\sigma ,$$

and

$$\log R = \frac{2\,u_p}{r}\, t + \log R_\sigma \qquad \text{(A.11)}$$

Appendix B

CALCULATION OF UNLOADING STRESS STATES

If both materials behave elastically in an asymmetrical impact, then from conservation of momentum across the shock front in each, the stress in each is readily obtained:

$$\sigma_t = k_1 u_p \qquad (1)$$

$$k_1 = \rho_o U_s$$

in the case of the target material and

$$\sigma_i = k_2 (V - u_p) \qquad (2)$$

$$k_2 = \rho_o U_s$$

in the impacting plate, where u_p is particle velocity, v is the impacting velocity, and k is the product of initial density and shock velocity, which remains constant. Successive reverberations of the unloading wave in the impacting plate result in a series of common decreasing stress steps at the interface of the two materials. These states are represented by σ_b, σ_c, σ_d, σ_e, and so forth, of Fig. A1, and σ_a in the initial impact stress. Corresponding particle velocity states are u_a, u_b, u_c, and so forth. Values of free-surface velocity of the impacting plate are v_1, v_2, v_3, and so forth. Since the stress and particle velocity across the interface are equal as long as the stress remains compressive and the flow is plane, then the above equations can be solved simultaneously, giving:

$$u_{p_a} = V\left(\frac{k_2}{k_1 + k_2}\right) \qquad (3)$$

and

$$\sigma_a = V\left(\frac{k_1 k_2}{k_1 + k_2}\right) \qquad (4)$$

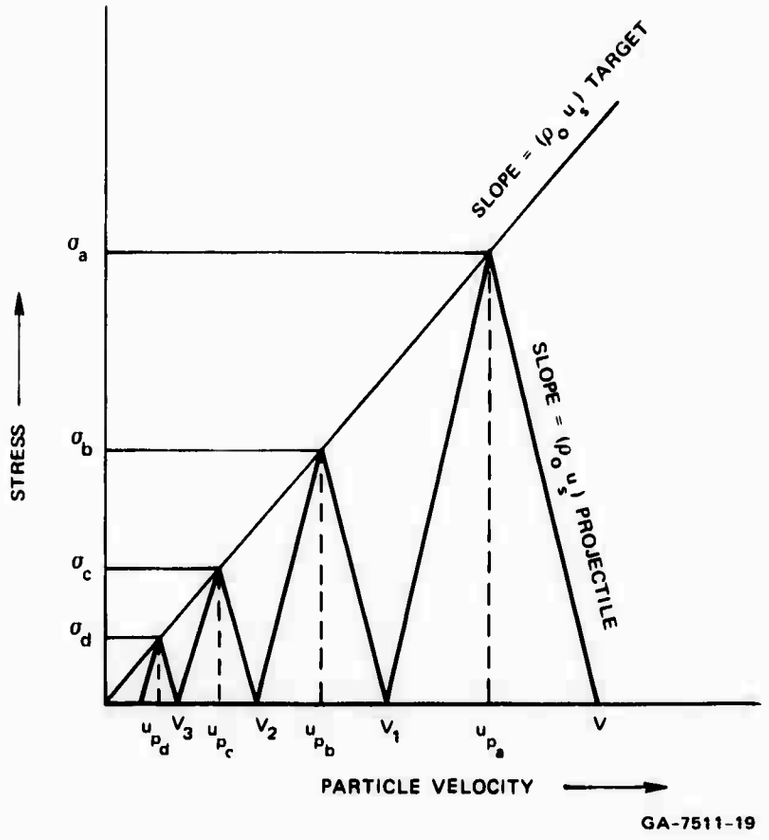

FIGURE B.1 SUCCESSIVE STRESS-PARTICLE VELOCITY STATES OBTAINED FROM ASYMMETRICAL IMPACT OF TWO ELASTIC MATERIALS

The value of σ_b is obtained similarly from:

$$\sigma_b = k_1 u_{pb} = k_2 (v_1 - u_{pb}) \tag{5}$$

where

$$v_1 = v - 2 (v - u_{pa}) \tag{6}$$

$$= 2u_{pa} - v$$

Therefore,

$$\sigma_b = k_2 [(2 u_{pa} - v) - u_{pb}] \tag{7}$$

and

$$u_{pb} = \frac{k_2}{k_1 + k_2} (2 u_{pa} - v) \tag{8}$$

since

$$u_{pa} = \frac{k_2}{k + k_2} v \tag{9}$$

$$\sigma_b = \frac{vk_1k_2}{k_1 + k_2} (2 \frac{k_2}{k_1 + k_2} - 1) \tag{10}$$

That is

$$\sigma_b = \sigma_a (2 \frac{k_2}{k_1 + k_2} - 1) \tag{11}$$

Similarly, successive unloading stresses are given by

$$\sigma_c = \sigma_b (2 \frac{k_2}{k_1 + k_2} - 1) \tag{12}$$

$$\sigma_d = - - - - - \tag{13}$$

BLANK PAGE

Appendix C

CORRECTION TO V/V_o DATA DUE TO RESISTANCE OF VOLTAGE LEADS

In configuration 1 of the test samples (Figure 4.1 in text) the π pattern is roughly symmetrical, i.e., the resistances between an extremity and junction are approximately equal and all are a function of stress. If a constant current supply is used to power the resistance film, the change in resistance of the current portion of the π does not affect the measurement of the change in resistance. The change in resistance of the voltage legs will, however, greatly affect the observed ratio of $\Delta V/V$, if the resistance of the legs is an appreciable percentage of the total resistance in the voltage circuit. In configuration 1, lead resistances amounted to as much as 6% of the voltage leg resistance. Since ytterbium exhibits changes of resistance of up to 5 fold on shock loading, the 6% amounts to 30% at peak stress. A correction was made as follows.

In the circuit of Figure C-1, r_1 is the total resistance of the ytterbium voltage leads, $r_2 = r_3 = 50\ \Omega$, V is voltage across the "active" portion of the gage, r_g, and E the measured voltage. The initial value of E is

$$E_o = \frac{r_3}{r_1 + r_2 + r_3} \quad V_o \tag{C.1}$$

and at pressure P is

$$E_p = \frac{r_3}{r_{1_p} + r_2 + r_3} \quad V_p \tag{C.2}$$

but

$$r_{1_p} = \frac{V_p}{V_o} \times r_1 \tag{C.3}$$

Preceding page blank

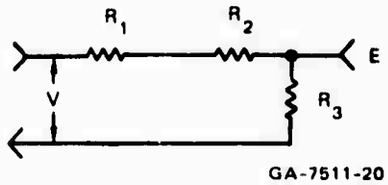

FIGURE C.1 GAGE AND SHUNT RESISTANCE CIRCUIT

since both resistances are ytterbium. Therefore

$$\frac{E_p}{E_o} = \frac{V_p}{V_o} \frac{(r_1 + r_2 + r_3)}{\frac{V_p}{V_o} r_1 + r_2 + r_3} \tag{C.4}$$

or

$$\frac{V_p}{V_o} = \frac{(r_2 + r_3)\, E_p/E_o}{r_1 \left(1 - \frac{E_p}{E_o}\right) + r_2 + r_3} \tag{C.5}$$

The change in r_1 also results in a change in the resistance r_g due to the shunting effect of $r_1 + r_2 + r_3$. However for typical values of $r_g = 1\ \Omega$, $r_1 \sim 3\ \Omega$, and $r_2 = r_3 = 50\ \Omega$, this effect is negligible.

Curves of V_p/V_o versus r_p/r_o for three cases are shown in Figure C-2: (1) a one-to-one correspondence between V_p/V_o and r_p/r_o, i.e., $r_1 = 0$, $r_2 + r_3 = \infty$; (2) $r_g = 1\ \Omega$, $r_1 = 1\ \Omega$, $r_2 = r_3 = 50\ \Omega$; and (3) $r_g = 1\ \Omega$, $r_1 = 5\ \Omega$, $r_2 = r_3 = 50\ \Omega$. Case (2) applied to the majority of measurements made with configuration 1.

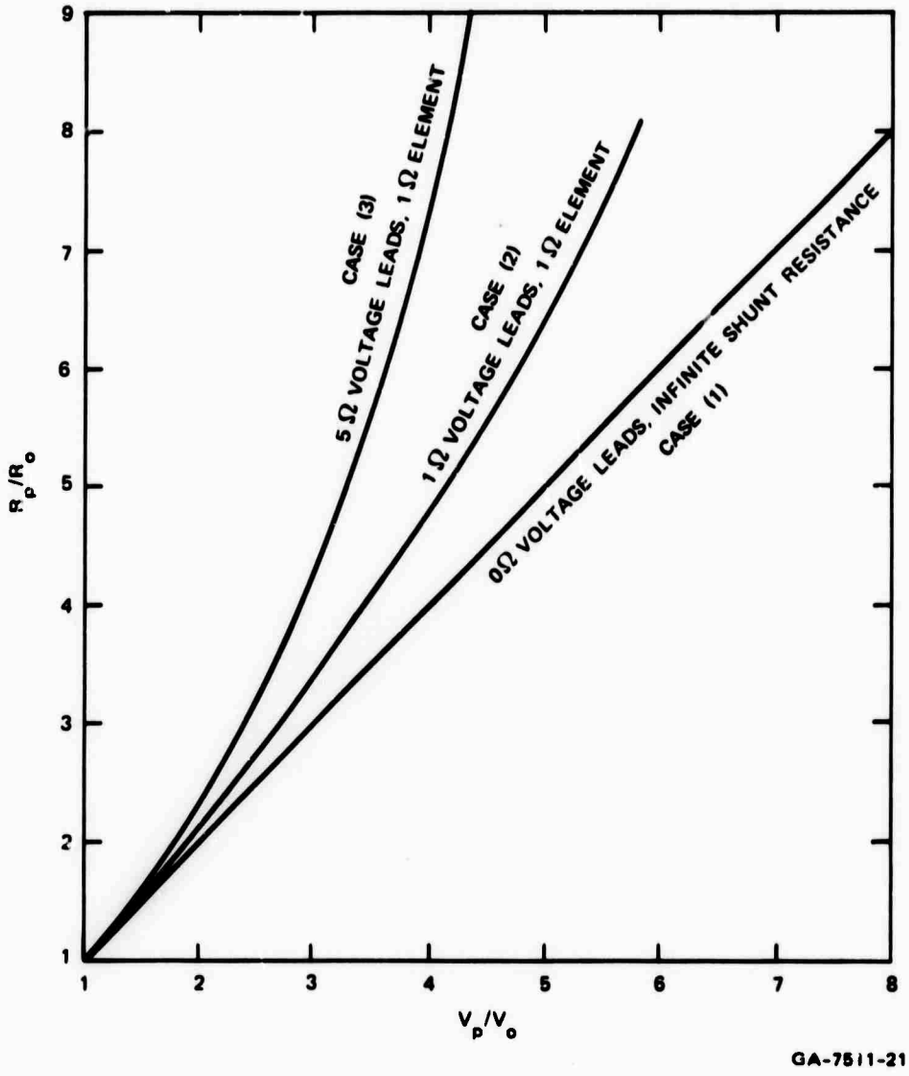

FIGURE C.2 OBSERVED VOLTAGE CHANGE VERSUS ACTUAL RESISTANCE CHANGE

REFERENCES

1. D. D. Keough, "Pressure Transducer for Measuring Shock Wave Profiles--Phase IX: Additional Gage Development," Final Report, Stanford Research Institute, Contract No. DA-49-146-XZ-096, November 1964.
2. D. D. Keough and W. Wilkinson, "Development of Pressure Gages for Project Piledriver," Final Report, Stanford Research Institute, Contract No. DA-49-146-XZ-280, February 1967.
3. F. M. Sauer, C. T. Vincent, R. C. Kiessling, and H. G. Hucback, "Close-In Earth Motion Studies/Pressure Measurements in the Hydrodynamic Region," POR-3016, Stanford Research Institute, Contract No. DA-49-146-XZ-345, December 1967.
4. F. M. Sauer and C. T. Vincent, "Earth Motion and Pressure Histories," POR-3002, Stanford Research Institute, Contract No. DA-49-146-XZ-207, April 1967.
5. C. T. Vincent, "Project 3.04b, Event 3, Close-In Shock Profile Studies," Operation Distant Plain Symposium, DAIAC Special Report SR-60, September 1967, pp. 466-501.
6. F. M. Sauer, B. Barclay, C. T. Vincent, and J. R. Rempel, "Earth Pressure and Motion Measurement (S-RD)," Draft POR-3027, Stanford Research Institute, Contract No. DA-49-146-XZ-371, February 1967.
7. C. T. Vincent, "Stemming and Containment Diagnostics (S-RD)," Draft POIR, Stanford Research Institute, Contract No. DASA-01-167-C0068, January 1968.
8. C. T. Vincent, "Stemming and Containment Diagnostics (Confidential)," Draft POR, Stanford Research Institute, Contract No. DASA-01-67-C0053, January 1968.
9. P. Lieberman, "Close-In Pressure-Time Histories for the Flat Top Experiments," IIT Research Institute, December 1964.
10. R. F. Williams, "Pressure Transducer for Measuring Shock Wave Profiles--Phase X: Measurement of Low Pressure," Final Report, Stanford Research Institute, Contract No. DA-49-146-XZ-096, May 1965.
11. D. D. Keough, R. F. Williams, and R. A. Pasternak, "Piezoresistive Shock Transducer Study Using Lithium," Final Report, Stanford Research Institute, Sandia Contract 18-5816, August 12, 1968.

REFERENCES (contd)

12. P. W. Bridgman, "Effects of Pressure on Binary Alloys," Proc. Amer. Acad. Arts Sci. 83(5), 156 (September 1954).
13. R. F. Williams, "Development of a Lithium Pressure Gage," Final Report, Stanford Research Institute, Sandia Contract 20-7694, August 15, 1969.
14. H. T. Hall and L. Merrill, Inorg. Chem. 2, 618 (1963).
15. D. B. McWhan, T. M. Rice, and P. H. Schmidt, Phys. Rev. 3, 177 (1969).
16. P. W. Bridgman, "The Resistance of Nineteen Metals to 30,000 Kg/cm^3," Proc. Am. Acad. Arts Sci. 72, 157-205 (1938).
17. M. McKay, "Spherical Wave Propagation in Earth Materials," DASA 2128, Proceedings: Strategic Structures Vulnerability/Hardening Long Range Planning Meeting, Vol. I. DASIAC Special Report 85, June 1969.
18. S. Rubin et al., "Output Diagnostics for Door Mist," POR, Stanford Research Institute, DASA Contract 01-67-C-0057, December 1968, Draft.
19. R. K. Linde and D. N. Schmidt, Rev. Sci. Instr. 37, 1 (1966).
20. G. R. Fowles, "Shock Wave Compression of Hardened and Annealed 2024 Aluminum, J. Appl. Phys. 32, 1475-1487 (1961).
21. T. J. Ahrens, W. H. Gust, and E. B. Royce, J. Appl. Phys. 39, 4610 (1968).
22. C. F. Petersen, W. J. Murri, and M. Cowperthwaite, "Hugoniot and Release Adiabat Measurements for Selected Geologic Materials," J. Geophys. Res., in press.
23. Handbook of Chem. Phys., 48th Ed., R. C. Weast, S. M. Selby, eds., Chemical Rubber Company, 1968, p. F133.
24. H. D. Stromberg and D. R. Stephens, J. Phys. Chem. Solids 25, 1015-1022 (1964).
25. J. Y. Wong and P. S. De Carli, "The Effects of Shock Waves on Meteorites," Final Report, Stanford Research Institute, Contract NASr-49(24), June 30, 1968.
26. W. Boas, "Stored Energy and Lattice Defects in Cold-Worked Metals," Proc. Conference on Defects in Crystalline Solids, The Physical Society, London, July 1954.

27. M. H. Rice, R. G. McQueen, and J. M. Walsh, Solid State Physics (Academic Press, New York, 1958), Seitz and Turnbull, eds., Vol. 6.

28. P. J. A. Fuller and J. H. Price, Brit. J. Appl. Phys. 15, 751 (1964).

UNCLASSIFIED

Security Classification

DOCUMENT CONTROL DATA - R & D

(Security classification of title, body of abstract and indexing annotation must be entered when the overall report is classified)

1. ORIGINATING ACTIVITY (Corporate author)	2a. REPORT SECURITY CLASSIFICATION
Stanford Research Institute 333 Ravenswood Avenue Menlo Park, California 94025	UNCLASSIFIED 2b. GROUP

3. REPORT TITLE

DEVELOPMENT OF A HIGH-SENSITIVITY SHOCK TRANSDUCER FOR THE LOW KILOBAR RANGE

4. DESCRIPTIVE NOTES (Type of report and inclusive dates)

FINAL REPORT - March 1970

5. AUTHOR(S) (First name, middle initial, last name)

Douglas D. Keough

6. REPORT DATE	7a. TOTAL NO. OF PAGES	7b. NO. OF REFS
March 25, 1970	102	26

8a. CONTRACT OR GRANT NO.	9a. ORIGINATOR'S REPORT NUMBER(S)
DASA-69-C-0014 b. PROJECT NO. ARPA ORDER 1238 PC 8F10 c. Program Code 7B42-71107 d.	PYU 7511 9b. OTHER REPORT NO(S) (Any other numbers that may be assigned this report) DASA 2508

10. DISTRIBUTION STATEMENT

This document has been approved for public release and sale; its distribution is unlimited.

11. SUPPLEMENTARY NOTES	12. SPONSORING MILITARY ACTIVITY
	Advanced Research Project Agency Department of Defense Washington, D.C. 20301

13. ABSTRACT

The shock piezoresistance response of two metals, ytterbium and bismuth, was investigated--ytterbium over a range from 4 to 40 kbar and bismuth at 10 and 20 kbar. The sensitivity of both materials at a few kilobars is approximately 12 times that of manganin and both show nonlinear, monotonically varying resistance-stress behavior. Unloading response was measured at from 10 and 20 kbar in ytterbium and found to be nonlinear at the higher range. A positive residual resistance was measured which was essentially independent of peak stress. A system consisting of the impact of two elastic materials was developed for the measurement of hysteresis. Comparison of static and dynamic piezoresistance data indicates that the difference between the two is too large to be attributed to temperature and geometrical considerations. Although it may be due to defect production, this phenomenon was not investigated specifically. Results with manganin, foils and wires, however, did show a difference in certain insulators which is attributed to defect production. Foils approximately 0.013 mm thick and films approximately 0.6 μ thick were constructed readily from bulk ytterbium. Bismuth films were constructed from bulk bismuth by vapor deposition. Long-time-duration recording was achieved by bonding ytterbium foils between wafers of polycrystalline aluminum oxide. A duration of ~ 30 μsec at a stress of 10 kbar was achieved in experiments with the SRI 4-inch barrel diameter gas gun. Reduction in foil elongation and hence a reduction in sensitivity to lateral stress disturbances appears to be due to the encapsulation of the foil in high-modulus, high-shock-impedance insulators.

DD FORM 1 NOV 68 1473 (PAGE 1)

S/N 0101-807-6801

UNCLASSIFIED

Security Classification

14 KEY WORDS	LINK A		LINK B		LINK C	
	ROLE	WT	ROLE	WT	ROLE	WT
Shock transducer						
Piezoresistance						
Ytterbium						
Bismuth						
Divergent flow						